HHS Public Access

Author manuscript

Nat Cancer. Author manuscript; available in PMC 2021 September 01.

Published in final edited form as:

Nat Cancer. 2021 March ; 2(3): 300–311. doi:10.1038/s43018-021-00180-1.

Resident and circulating memory T cells persist for years in melanoma patients with durable responses to immunotherapy

Jichang Han[1], **Yanding Zhao**[2], **Keisuke Shirai**[3,5], **Aleksey Molodtsov**[1], **Fred W. Kolling**[3], **Jan L. Fisher**[5], **Peisheng Zhang**[3], **Shaofeng Yan**[6], **Tyler G. Searles**[3], **Justin M. Bader**[3], **Jiang Gui**[3], **Chao Cheng**[7], **Marc S. Ernstoff**[8], **Mary Jo Turk**[1,3,*], **Christina V. Angeles**[3,4,9,*]

[1]Department of Microbiology and Immunology, The Geisel School of Medicine at Dartmouth, Lebanon, NH, 03756

[2]Department of Molecular and Systems Biology, The Geisel School of Medicine at Dartmouth, Lebanon, NH, 03756

[3]Department of Norris Cotton Cancer Center, The Geisel School of Medicine at Dartmouth, Lebanon, NH, 03756

[4]Department of Surgery, Dartmouth-Hitchcock Medical Center, Lebanon, NH 03756

[5]Department of Medicine, Dartmouth-Hitchcock Medical Center, Lebanon, NH 03756

[6]Department of Pathology, Dartmouth-Hitchcock Medical Center, Lebanon, NH 03756

[7]Baylor School of Medicine, Houston, TX 77030

[8]Roswell Park Cancer Institute, Buffalo, NY 14263

Corresponding Authors: Mary Jo Turk, PhD, Geisel School of Medicine at Dartmouth, One Medical Center Drive, Lebanon, NH 03756, 603-653-3549, mary.jo.turk@dartmouth.edu, Christina V. Angeles, MD, University of Michigan, Rogel Cancer Center, 1500 E. Medical Center Drive, 6219 Cancer Center, Ann Arbor, MI 48109, 734-615-4823, angelesc@med.umich.edu.

*equal contribution

Author Contributions

CVA and MJT conceived and supervised the study. JH, MJT, and CVA drafted the paper and figures. JH and YZ carried out the primary analysis. CVA, MSE, and KS carried out patient recruitment. JH, JLF, PZ, and TGS processed tissues and carried out flow cytometry and FACS. JH and TGS extracted the DNA for bulk TCR sequencing. SY provided dermatopathology expertise and assisted with IHC analysis. FWK carried out scRNA and scTCR library preparation and sequencing. CC, YZ, and AM provided bioinformatic support. CVA, KS and JB collated the clinical data. JG provided statistical support. MJT provided scientific and infrastructural support. All authors reviewed and edited the final paper.

Competing Interests Statement

All authors declare no competing interests.

Data availability

Single-cell RNA-seq and TCR-seq data that support the findings of this study have been deposited in the database of Genotypes and Phenotypes (dbGaP) under the accession code phs002309.v1.p1. Bulk TCRseq data can be accessed through the ImmuneACCESS database of Adaptive Biotechnologies (https://doi.org/10.21417/JH2021NC; https://clients.adaptivebiotech.com/pub/han-2021-natcancer). The published microarray datasets used to generate the comprehensive $CD8^+$ T_{RM} signature for the GSEA analysis were accessible at Gene Expression Omnibus (GEO) under accession codes GSE47045, GSE15907 and GSE37448. The remaining gene sets used in the GSEA analysis were accessible through the MSigDB database (https://www.gsea-msigdb.org/gsea/msigdb). The published TCGA skin cutaneous melanoma (SKCM) RNA-seq data used to perform the survival analysis is available at Firehose (http://gdac.broadinstitute.org/). Two additional previously published stage III/IV melanoma patient RNA-seq datasets are available at the GEO database with the following accession numbers: GSE54467, GSE19234. Source data are available for this study. All other data supporting the findings of this study are available from the corresponding author on reasonable request.

Code availability

The open source code is available at GitHub. Codes for gene expression analyses including single cell RNA-seq data analysis, survival analysis, GSEA analysis are publicly available on GitHub (https://github.com/TrmMelanoma/Gene-expression-related-analysis). Codes for TCR analyses including single cell TCR-seq data analysis and bulk TCR-seq data analysis are publicly available on GitHub (https://github.com/TrmMelanoma/TCR-analysis).

[9]University of Michigan Rogel Cancer Center, University of Michigan, Ann Arbor, MI 48109; Department of Surgery, University of Michigan, Ann Arbor, MI 48109

Abstract

While T-cell responses to cancer immunotherapy have been avidly studied, long-lived memory has been poorly characterized. In a cohort of metastatic melanoma survivors with exceptional responses to immunotherapy, we probed memory $CD8^+$ T-cell responses across tissues, and across several years. Single-cell RNA sequencing revealed three subsets of resident memory T (T_{RM}) cells shared between tumors and distant vitiligo-affected skin. Paired T-cell receptor sequencing further identified clonotypes in tumors that co-existed as T_{RM} in skin and as effector memory T (T_{EM}) cells in blood. Clonotypes that dispersed throughout tumor, skin, and blood preferentially expressed a *IFNG* / *TNF*-high signature, which had a strong prognostic value for melanoma patients. Remarkably, clonotypes from tumors were found in patient skin and blood up to nine years later, with skin maintaining the most focused tumor-associated clonal repertoire. These studies reveal that cancer survivors can maintain durable memory as functional, broadly-distributed T_{RM} and T_{EM} compartments.

Metastatic melanoma (MM) patients can develop durable responses to immunotherapy[1–3], however, the underlying mechanisms are not well understood. While previous studies have identified predictors of immediate T-cell responses by examining the blood and tumor infiltrating lymphocytes (TILS) from patients on immunotherapy[4–7], subsets of long-lived memory T cells have yet to be thoroughly investigated. Of melanoma patients who receive immunotherapy, long-term survivors are frequently found to develop melanoma-associated vitiligo, an autoimmune cutaneous side effect[8–10]. Vitiligo may serve as a key determinant of survival in patients, as studies in mouse models have shown that this autoimmune condition sustains $CD8^+$ T-cell memory to melanoma[11]. We postulated that the study of vitiligo-affected melanoma patients with exceptional responses to immunotherapy would provide novel insights into the localization, persistence, and function of durable memory T-cell responses to cancer.

Matched melanoma tumor, distant vitiligo-affected skin, and blood were collected at least twelve months after initiation of a variety of immunotherapy regimens, and at least one month after therapy completion, from four long-term MM survivors (PT615, PT625, PT628, and PT635; Supplementary Table 1, Extended Data Fig. 1). In these patients, biopsied tumors were found to be either stable or regressed, as potential evidence of a protective immune response. $CD45^+CD8^+$ T cells from specimens were isolated by fluorescence-activated cell sorting (FACS) prior to parallel single-cell RNA (scRNA-seq) and T-cell receptor (TCR) sequencing (scTCR-seq) (Fig. 1a, Extended Data Fig. 2). In total, scRNA-seq data were obtained from 12,777 $CD8^+$ T cells with paired TCR sequences in 10,658 cells (83%; Supplementary Table 2–3). Gene expression data analyzed by Seurat 3.0 showed that T-cell transcriptional clustering was dictated by specimen type rather than patient-specific variances (Fig. 1b). Notably, transcriptional profiles of $CD8^+$ T cells from skin and tumor specimens were highly overlapping, showing high expression of resident memory T-cell (T_{RM})-related transcripts including *CD69* and *RGS1*, which was in contrast to high levels of circulating T-cell associated transcripts *S1PR1* and *SELL* in blood (Fig. 1b–c).

Flow cytometry from a similar patient cohort confirmed a $CD69^{hi}$ $CD62L^{low}$ phenotype of $CD8^+$ T cells in skin, but not in blood (Extended Data Fig. 1 and Extended Data Fig. 3a–b), and immunohistochemistry further confirmed the infiltration of $CD69^+CD8^+$ cells throughout the dermis and epidermis of skin (Extended Data Fig. 3c).

Unsupervised clustering of $CD8^+$ T cells from scRNA specimens identified ten distinct transcriptional clusters (C1–10; Fig. 1d). With the exception of C4, all clusters were comprised of cells from all patients (Extended Data Fig. 4). Clusters C1-C5 consisted overwhelmingly of T cells from blood, with features of effector memory (C1-T_{EM}) (low *SELL* and *CCR7,* but high *CX3CR1*)[12,13], effector (C2-T_{EFF}) (high *GNLY*, *GZMB*, and *PRF1*)[14,15], central memory (C3-T_{CM}) (high *SELL*, *IL7R*, and *CCR7*)[13,16], naïve (C4-T_{NAV}) (high *CCR7*, *TXNIP*, and *PIK3IP1*)[13,17,18], and mucosal-associated invariant T cells (C5-MAIT)[19], respectively. Cluster C6 (C6-Skin T cells), comprised solely of T cells from skin, was mainly differentiated by high expression of *LGALS1 and VIM* (both adhesion molecules[20]), whereas C7, comprised solely of T cells from tumors, expressed high *TCF7*, *SELL, and CD27,* consistent with the phenotype of stem cell memory (C7-T_{SCM}) cells[21,22]. Importantly, clusters C8-C10, were each comprised of a mixture of T cells from skin and tumor, and each expressed high levels of T_{RM}-associated transcripts[23] including *CD69*, *RGS1, NR4A1 and CXCR6 (*Fig. 1e–f, Supplementary Table 4). *ZNF683 (HOBIT)* was not found, consistent with a prior study involving human T_{RM} cells[24]. Thus, tumor and skin both contained $CD8^+$ T_{RM} clusters which were discrete from T_{SCM} cells.

The identification of $CD8^+$ T_{RM} cells as a heterogenous population is consistent with a recent report that T_{RM} cells can adopt different transcriptional states[25], however, the key defining features of these subsets remained poorly characterized. Based on a core T_{RM} gene set that differentiated skin T_{RM} cells from other $CD8^+$ (non-T_{RM}) subsets (see Methods), gene set enrichment analysis (GSEA) revealed significant enrichment of T_{RM} transcriptional features in clusters C8, C9, and C10, but not in other clusters (Fig. 2a, Extended Data Fig. 5a). Moreover, two additional consensus T_{RM} gene lists - human cancer infiltrating T_{RM}[25] and mouse skin/gut/lung T_{RM}[26] - were found to be specifically enriched in the transcriptional profiles of clusters C8-C10 (Extended Data Fig. 5b–d), further validating that these populations were T_{RM} cells. However, each cluster also had unique defining features. Cluster C8 (designated C8-T_{RM}-FOS) expressed high levels of transcripts indicative of TCR signaling (i.e. *FOS, JUN, and NR4A1)*, whereas C9 (designated C9-T_{RM}-IFNG) was defined by high expression of several cytokines and chemokines (e.g. *IFNG, TNF*, *CCL3*, and *CCL4)*. By contrast, cluster C10 (designated C10-T_{RM}-TOX) exhibited high transcripts for negative checkpoint/exhaustion markers (*TOX*, *LAG3*, *PDCD1* and *CTLA4),* as well as high *PRF1*, *GZMB, PRDM1* (encodes BLIMP1) and *ITGAE* (encodes CD103) (Fig. 2b). The expression of CD103 by only a minor subset of T cells in skin was confirmed by flow cytometry (Extended Data Fig. 3b), and is in accordance with a prior report that $CD103^-CD69^+$ T_{RM} cells are the prevalent population in the dermis of vitiligo-affected skin[27]. Of note, the C10-T_{RM}-TOX transcriptional profile was found to be highly overlapping with a melanoma-infiltrating dysfunctional $CD8^+$ gene signature[28] (Extended Data Fig. 5e), consistent with recent studies in multiple cancer types that tumor infiltrating $CD8^+$ T_{RM} cells are a heterogenous population, including subsets with features of exhaustion.[15,29] Therefore, apart from previously described $CD103^+$ $CD69^+$ PD1-expressing

[25,29] T_{RM} cells, other transcriptionally distinct T_{RM} subsets were prevalent in patient melanomas.

To determine the potential prognostic values of these T_{RM} sub-populations, subset-defining transcriptional signatures were used to determine enrichment scores in MM specimens based on data from The Cancer Genome Atlas (TCGA). Enrichment of the C9-T_{RM}-IFNG signature was a significant predictor of patient overall survival, even when adjusting for overall T-cell infiltration, and numerous clinical variables (Fig. 2c–d, Extended Data Fig. 6). The C10-T_{RM}-TOX signature also held prognostic value as a single variable, however C8-T_{RM}-FOS did not (Fig. 2c, Extended Data Fig. 6). Thus, C9-T_{RM}-IFNG cells are a highly prognostic subset that is present in both tumor and skin of long-term melanoma survivors.

Transcriptional profiling revealed clear differences between circulating T cells and those resident in tissue. However, it remained unknown how individual T-cell clones behaved across compartments and transcriptional clusters. Thus, paired scTCR-seq data were analyzed from four patients (PT615, PT625, PT628, PT635; Supplementary Table 5). Gini index indicated similar baseline clonal expansion levels across the three T_{RM} clusters (Extended Data Fig. 7a). Focusing on clones that had expanded (>2 cells) in tumor specimens, as a reference for “tumor-associated” clonotypes that may participate in anti-tumor immunity, we identified a total of thirty-three tumor-associated clonotypes containing counterparts in skin across four patients (Fig. 3a, Extended Data Fig. 7b). Of these tumor/skin clonotypes, fifteen had cell counterparts that could be identified in the blood – designated “Resident/Circulating”, whereas eighteen did not – “Resident-Only” (Fig. 3b, Extended Data Fig. 7c–d). Eleven additional tumor-associated clonotypes were identified in the blood, but not found in the skin, and accordingly deemed “Circulation-Capable” clonotypes (Fig. 3b, Extended Data Fig. 7e). Thus, with the caveat that incomplete sampling could give the appearance of cells as being excluded from a given compartment, distinct clonotypes were found to have propensity for different tissue locations.

To explore potential differences in transcriptional features of these three clonal categories, we generated an ‘Enrichment_Score’ (Methods) to evaluate the cluster enrichment of each subset. T cells belonging to Resident/Circulating clonotypes were found to be significantly enriched in the highly prognostic C9-T_{RM}-IFNG cluster, regardless of whether they had derived from skin or tumor specimens. This suggests that these location-promiscuous clonotypes were transcriptionally stable as functional C9-T_{RM}-IFNG cells even in tumors. Furthermore, these clonotypes were significantly enriched in the C1-T_{EM} cluster when identified in blood, supporting the existence of a common clonal precursor for skin T_{RM}, tumor T_{RM}, and blood T_{EM} cells in melanoma survivors. In contrast, T cells belonging to the Resident-Only and Circulation-Capable subtypes tended to be more enriched in the C10-T_{RM}-TOX cluster when in tumors (Fig. 3c). Interestingly, “Resident/Circulating” clonotypes tended to have the highest overall frequencies (Fig. 3d), suggesting, in parallel, that highly expanded clonotypes were more likely to be C9-T_{RM}-IFNG cells.

Given the fact that Resident/Circulating clonotypes were expanded in tumor and also present in vitiligo-affected skin, we expected some to have specificity for melanoma differentiation antigens (MDAs)[30]. Known MDA (MART-1, gp100, and tyrosinase) specificity was tested

by dextramer staining of blood and skin samples from a separate cohort of five metastatic melanoma survivors with immunotherapy-associated vitiligo and identified MDA-specific responses in both skin and blood (Fig. 4a–b). In one patient, longitudinal blood specimens were analyzed, and remarkably, the MART-1 specific population remained capable of IFNγ secretion for a period of at least six years (Fig. 4c–d). These results demonstrate the development of functional, durable, tumor/self-antigen-specific memory in long-term melanoma survivors.

To quantitatively assess the long-term persistence of tumor-associated T-cell clonotypes in patients, bulk TCRβ DNA sequencing (Adaptive Biotechnologies) was performed on skin, blood, and archival primary and metastatic tumors from seven long-term melanoma survivors (PT601, PT604, PT612, PT625, PT626, PT628, and PT635; Fig. 5a, Methods). Indeed, early tumor-associated T-cell clonotypes were identified as persisting in the skin and blood of all patients. Most strikingly, multiple clones persisted six, eight, and even nine years after tumor excision, as definitive evidence of durable memory (Fig. 5b, Extended Data Fig. 8, Supplementary Table 6). Since tumor-matched clonotypes in the blood of melanoma patients are associated with response to immunotherapy[31–33], the clonal match index was compared between tumor and blood vs. tumor and skin of each patient (Fig. 5c). Compared with blood, the skin maintained a significantly more focused tumor-associated TCR repertoire, indicating a unique role for skin in sustaining anti-melanoma immunity (Fig. 5d).

To better understand the behaviour of these long-lived tumor-associated clonotypes, their expansion in skin and blood, at least 3 years after tumor removal, was assessed. Indeed, persisting tumor-associated clonotypes that had clonally expanded in the skin were also more clonally expanded in blood, supporting the notion that skin T_{RM} clonotypes comprise a more robust host-wide memory response than clonotypes that are not capable of skin residence (Fig. 6a). To investigate the transcriptional properties of these long-lived clonotypes, data from TCR DNA sequencing were aligned to the scTCR-seq dataset. One patient (PT635) had both archival tumor and optimal scTCR-seq data which enabled matching of four tumor-associated clonotypes that had persisted in skin and blood for six years (Fig. 6b, Methods). Transcriptional analysis of these clonotypes demonstrated that they persisted exclusively as $CD8^+$ C9-T_{RM}-IFNG cells in skin, and preferentially as C1-T_{EM} cells in blood (Fig. 6b–c), revealing that truly long-lived memory responses in melanoma survivors develop into functional T_{RM} and T_{CIRCM} compartments.

In summary, we demonstrate that tumor-associated T cells can commit to multiple memory lineages in cancer survivors, producing durable, systemic, and functional immunity. Although the protective function of memory T cells in human cancers has been proposed, prior studies have not addressed T-cell long persistence[15,29,34]. We reveal that both skin and blood of long-term MM survivors are capable of sustaining tumor-associated T-cell clones for durations of up to nine years. Building on prior reports that T_{RM} cells are associated with improved patient survival[29,35], we further highlight C9-T_{RM}-IFNG cells as the most long-lived, functional, and prognostic subset. This supports a large body of work identifying IFNγ as a predictor of patient survival and mediator of tumor elimination[36–39]. These long-persisting C9-T_{RM}-IFNG cells in skin and tumor appear to arise from the same clonal

precursor as T_{EM} cells in blood, which is consistent with the ontogeny of T_{RM} and T_{CIRCM} cells in mouse viral infection models[40–42]. While we identified functional, long-lived MART-1-specific populations in survivors with vitiligo, additional work will be required to identify the target antigens of Resident/Circulating clonotypes more broadly, with a focus on neo-antigens as important targets for cancer immunity[43,44]. Since T_{RM} cells are known to be present in pre-treatment tumors[25], future studies should also address how immunotherapy and/or vitiligo development affect the phenotype and clonal expansion of such pre-existing populations. Further investigation of long-lived, widely dispersed T cells in patients who achieve exceptional responses to immunotherapy, should guide perspectives on what constitutes curative immunity to cancer.

METHODS

Sample collection:

IRB-approved written informed consent was obtained from patients with advanced melanoma, to perform skin and tumor biopsies, draw blood, and to access historical banked tissue and blood samples for analysis. All human studies were performed in accordance with ethical regulation, and pre-approved by the Committee for the Protection of Human Subjects at Dartmouth-Hitchcock Medical Center IRB (#00029821). This was not a prospective study. Advanced melanoma patients were recruited if they had an outstanding clinical response to immunotherapy as evidenced by tumor regression and the development of vitiligo. Types of immunotherapy and timing of biopsies were thus varied among patients (Extended Data Fig. 1). Patients were selected for scRNA/TCR seq analysis (n=4 total) if they were able to provide fresh matched tumor, blood, and skin specimens. Patients were selected for flow cytometry analysis (n=5 total) if they were HLA-A2.1 positive, and able to provide fresh matched skin and blood specimens. When identifying patients for adaptive TCR sequencing (7 total), we selected 3 out of 4 scRNAseq patients, and 2 out of 5 flow cytometry patients, based on whether or not archival tumor specimens were available. We additionally identified two long-term melanoma survivors with vitiligo from whom we had archival tumor specimens and were able to acquire matched skin and blood specimens. All skin biopsies (3-cm ellipses) were taken at sites distal to (most times different extremities from) tumor sites; anatomical locations of biopsies are shown in Supplemental Table 1. Skin biopsies contained the pigmented/depigmented border of vitiligo-affected regions, as confirmed by a dermatopathologist. Metastatic melanoma tumors were biopsied in clinic (research-only) or taken from clinically indicated operative specimens (1-cm^2). 50–70ml blood was collected into sodium heparin tubes on same day as tissue biopsy. Previously banked tumors were stored as formalin fixed paraffin embedded (FFPE) blocks.

Tissue processing:

All specimens for a single patient were processed on the day of collection. Skin and tumor specimens were weighed, cut into pieces, and then minced with surgical scissors. Minced specimens were digested in 5ml RPMI-1640 (Hyclone) containing 1 mg/mL collagenase type II (Sigma, C6885) and 2 mg/mL of DNase I (Sigma, DN25). Digest proceeded in glass vials, with gentle stirring, at 37 °C for 1 hour, after which an equal volume of cold flow buffer (PBS+0.2% BSA) was added. Samples were then filtered through a 70 μm cell

strainer. The single cell suspension was centrifuged at 1,800 RPM for 10min and resuspended in flow buffer at a concentration of 1×10^7 cells/ml. Peripheral blood mononuclear cells (PBMCs) were isolated from whole blood using Ficoll density gradient centrifugation.

Fluorescence activated cell sorting (FACS):

Single cell suspensions underwent Fc block with Human TruStain FcX (Biolegend; 1:20 dilution) for 15min on ice. Samples were then stained with 1:100 dilutions of antibodies to CD45, CD8, and CD4 (BV421-conjugated anti-human CD45 mAb clone 2D1, FITC-conjugated anti-human CD4 mAb clone RPA-T4, and APC-conjugated anti-human CD8 mAb clone RPA-T8). Samples were stained in the dark for 30min on ice, washed twice with flow buffer, and resuspended in PBS + 0.04% BSA. Sorting was performed on BD FACSAria™ II sorter. $CD8^+CD45^+CD4^-$ and $CD4^+CD45^+CD8^-$ cells from the same specimen were sorted into the same well of a 96-well plate. Tumor and skin specimens were each sorted in their entirety, whereas PBMC sorting was terminated when the total number of sorted cells reached 50,000. All samples from a single patient were sorted on the day of specimen collection.

Single-cell RNA-seq and single-cell TCR V(D)J profiling:

Immediately following sorting, cells were placed on ice and counted on a Luna II automated cell counter (PBMC) or hemocytometer (skin and tumor). The cell concentration was used to calculate the volume of single cell suspension needed in the reverse transcription master mix, aiming to achieve approximately 3,000 cells for the PBMC sample and 6,000 cells for tumor and the skin samples. The RNA-seq library and V(D)J library for TCR-seq were generated using a Chromium Single Cell 5′ Library and Gel Bead Kit (10x Genomics), following the manufacturer's protocol. Briefly, following capture, emulsions containing droplet-encapsulated single cells were reverse transcribed and barcoded, emulsions broken, and barcoded cDNA amplified by PCR according to the 10x Genomics' V(D)J enrichment protocol. Amplified cDNA and TCR-specific libraries were prepared following the standard 10x procedure to generate libraries for Illumina sequencing. Samples were uniquely barcoded, pooled and sequenced across multiple Illumina NextSeq500 High Output runs to generate 50,000 and 5000 reads/cell for gene expression and TCR libraries, respectively. Paired end sequencing was performed using 26 cycles for read 1 to decode the 16bp cell barcode and 10bp UMI sequences, and 98 cycles for read 2 corresponding to the transcript sequence. Raw sequencing data were processed through the Cell Ranger v3.0 pipeline (10x Genomics) using human reference genome GRCh38 to generate gene expression matrices for single cell 5' RNA-seq data as well as fully reconstructed, paired TRA/TRB sequences from each single cell.

Single cell RNA-seq data preprocessing:

The unique molecular identifier (UMI) counts based gene expression matrix was processed using the R package-Seurat (version 3.1)[45,46]. To exclude low quality cells, those with less than 200 genes detected, or more than 10% mitochondrial genes, were filtered from the dataset. To remove potential multiplets, cells with a total number of UMI counts higher than 20,000 or a number of genes detected higher than 3000 were also removed. The nUMI of all

cells was normalized and scaled by a single command 'sctransform' in the Seurat package, which has been shown to preserve a sharper biological distinction compared to a standard normalization workflow[47]. To focus on the $CD8^+$ T-cell population, cells without *CD8A* expression were excluded which resulted in extracting a total of 12,777 CD8 expressing cells with 10,658 of these also having a paired TCR sequenced. These 10,658 cells were used for downstream analyses.

Principle component analysis and unsupervised clustering:

UMI count matrices of cells that passed previous filtering were normalized using the R function *SCTransform*. The 3,000 most variable genes were identified using the default parameter. Variable TCR and immunoglobulin genes were removed from the list of variable genes to prevent clustering based on variable V(D)J transcripts. Principle component analysis (PCA) was performed using the normalized expression of the variable genes. Clusters were identified using K-nearest neighbor (KNN) graph-based clustering, implemented in the R function FindNeighbors and FindClusters, on the basis of the first 15 principle components (PCs). The total percentage of variance included with the first 15 PCs was 64%. The first 15 PCs were proven to be the dominant PCs, as adding additional PCs to the analysis resulted in similar clustering. The same principle components were used to generate the UMAP projections for visualization.

Tissue distribution preference analysis:

Ro/e was calculated based on a previously published method[15] to indicate the tissue of origin for cells in each cluster. Ro/e was equal to $\frac{Nobserve}{Nexpect}$, with $N_{observe}$ being the number of cells in a cluster that originated from a certain tissue, and N_{expect} being the random expectation calculated by chi-squared test.

Identification of marker genes for each cluster:

Upregulated biomarker genes for each cluster were identified by analyzing differentially expressed genes relative to all other clusters, using the Wilcoxon rank sum test embedded in the function *FindAllMarkers* of the R package Seurat. P-values were corrected for multiple comparisons by the Bonferroni method. Genes with a log2 fold-change (log2FC) > 0.25 and adjusted p-value < 0.05 were considered cluster-specific marker genes.

Gene set enrichment analysis (GSEA):

Since skin is a proven conventional niche for T_{RM} cells, we defined a comprehensive skin $CD8^+$ T_{RM} signature (Supplementary Table 7) using three microarray datasets from the public Gene Expression Omnibus (GEO) database: the dataset GSE47045 which includes the microarray expression of mouse skin $CD8^+$ T_{RM} cells[26], and, as a reference for non-T_{RM} $CD8^+$ T-cell subsets, all the $CD8^+$ T-cell subset data from Immgen datasets GSE15907 and GSE37448 [48,49]. This approach enabled identification of a consensus gene list that differentiated skin T_{RM} $CD8^+$ T cells from other $CD8^+$ T-cell subsets. Human homologues of mouse genes were used. Quantile normalization[50] was applied to re-scale the expression profiles at the probe level across all three datasets, and ComBat (from the sva package)[51] was utilized to integrate expression data into a single meta-dataset. The $CD8^+$ T-cell subsets

in the metadata were median normalized such that each gene's expression value reflected its relative abundance in a given $CD8^+$ T-cell subtype[52]. Expression values then underwent Z-transformation to acquire a standard normal distribution, with $Z > 0$ indicating upregulation and $Z < 0$ indicating downregulation. Z-scores were converted into P-values, with the skin T_{RM} signature only including genes with P-values < 0.001. This gene signature was added to the 'c2.all.v6.2.symbols' gene sets collection from the MSigDB database[53,54] (modified C2 dataset) for GSEA analysis. Pre-ranked GSEA was performed using the GSEA_4.0.3 software. Genes of each cluster that were used for the analysis were identified using the *FindAllMarkers* function in Seurat with parameters of logfc.thereshold=0.01 and min.pct=0.01. The log_2FC value was used as the ranking metric.

Survival analysis:

The Cancer Genome Atlas (TCGA) dataset of metastatic skin cutaneous melanoma (SKCM) specimens and associated patient survival was used to evaluate the prognostic value of unique gene signatures derived from individual scRNAseq clusters. The gene expression data and the clinical data were downloaded from the Broad GDAC Firehose (https://gdac.broadinstitute.org). Two additional stage III/IV melanoma patient datasets available from the GEO database with the following accession numbers: GSE54467, GSE19234 were also involved in the analysis[55]. The average z-transformed expression values of marker genes from each cluster were used to generate T_{RM} scores, and Cox proportional hazard models were used to determine the association between each cluster-specific score and patient overall survival. Patient samples were dichotomized into two groups using the median score as the cutoff. A univariate Cox regression model was used to determine the association between each dichotomized T_{RM} score and patient survival. A multivariate Cox regression model was used to determine the individual contribution of T_{RM} scores on survival after adjusting for total T-cell infiltration level[56] and other confounding clinical variables including age and tumor stage. The Kaplan-Meier method was used to plot survival curves with significance estimated using the log-rank test, using the R package "survival".

Flow Cytometry and dextramer staining:

Samples from patients who were identified as having an HLA-A*0201 allele by the American Red Cross testing lab, were included in the flow cytometry and dextramer staining analyses. Single cell suspensions from blood and skin (as described above) were stained for viability with Zombie Yellow (Biolegend) in protein free PBS buffer for 30 min. Samples were blocked with human Cohn fraction IgG (20 μl per sample). Cells were then stained with 21 μl (7μl for each) pooled PE conjugated HLA-A*0201 dextramers for three MDA epitopes (MART-$1_{26–35}$ ELAGIGILTV, $GP100_{209–217}$ ITDQVPFSV, and $TYR_{368–376}$ YMDGTMSQV; ImmuDex) for 10 minutes at ambient temperature. In a separate well, cells were incubated with an irrelevant dextramer as a negative control. After dextramer pre-incubation, cells were stained with a panel of antibodies for 45min, rotating in the dark at 4°C. The antibodies used were: anti-CD45-BV395 (clone HI30), anti-CD3-Pacific Blue (clone UCHT1), anti-CD8-PerCP/Cy5.5 (clone RPA-T8), anti-CD62L-PE Cy7 (clone DREG-56), anti-CD103-APC (clone Ber-ACT8), and anti-CD69-APC/Cy7 (clone FN50). 10 μl per sample of Brilliant stain buffer plus (BD Biosciences) was used. Flow cytometry was performed on a Bio-Rad YETI cell analyzer and data were analyzed using Flowjo V10.

Immunohistochemistry (IHC):

Skin from the center of each patient's biopsy specimen was formalin-fixed and paraffin-embedded. Sections of 4μm thickness were prepared on slides, and air dried at room temperature. Slides underwent deparaffinized, antigen retrieval, and staining using the BOND RX Fully Automated Research Stainer (Leica Biosystems) using mouse anti-human anti-CD8 antibody (clone 4B11) and rabbit anti-human anti-CD69 antibody (clone EPR21814). Binding was visualized using the Leica Bond Dual Detection kit for Fast red via red precipitate from ChromPlex Kit 1 Bond for rabbit antibody and Vina Green HRP chromogen kit (Biocare) for mouse antibody, hematoxylin counterstain. The immuno-stained slides (5 slides/patient; 3 patients) were digitized at ×400 magnification and crop images were collected.

Enzyme-linked immune absorbent spot (ELISpot) assay:

Purified $CD8^+$ T cells from patient blood were analyzed by IFNγ ELISPOT (MABTECH), according to the manufacturer's instructions. Briefly, plates were coated with human IFNγ capture antibody and blocked with RPMI media containing 7% FBS. $CD8^+$ T cells were magnetically sorted from PBMCs (Miltenyi Biotec Inc, human $CD8^+$ T cell Isolation Kit) and added to wells at 3×10^5 cells/100ul/well. HLA-A2.1 transduced target cells (K562A2.1, a gift from Alan Houghton, MSKCC) were pulsed with MHC-I restricted peptides ($MART\text{-}1_{26–35}$ ELAGIGILTV, $GP100_{209–217}$ ITDQVPFSV, $TYR_{368–376}$ YMDGTMSQV; or no peptide for control), at 37ºC for 30 minutes, irradiated, and added to each well at 3×10^4 cells/50ul/well. Cells were incubated for 20h at 37°C, and ELISPOT was then developed with aminoethylcarbazole chromogen. Spots per well were counted on an automated reader system with KS 4.3 software (Carl Zeiss).

Single cell TCR-seq analysis:

TCR annotation was performed using the 10x cellranger vdj pipeline (10x Genomics), as described. For each sample, two output files were used for downstream analysis: Cell Ranger-filtered_contig_annotations.csv and clonotypes.csv. Each contained TCR α-chain and β-chain CDR3 nucleotide sequences for each single cell or fully constructed paired TCR α-chain and β-chain CDR3 nucleotide sequences for each TCR clonotype. Fully reconstructed, paired TCR α-chain and β-chain CDR3 nucleotide sequences were used to identify matched TCR clonotypes between tissues. Identical CDR3 nucleotide sequences for both TCR α-chain and β-chain were required for calling of matched TCR clonotypes. Matched TCR clonotypes with two or less cells in skin or tumor were excluded from the analysis to focus on clonally expanded TCR profiles.

Cell barcodes for matched TCR clonotypes were retrieved and matched to cell barcodes in the scRNA-seq dataset, such that cells with productive sequences for both TCR, and RNAseq could undergo further analysis. To evaluate if a given group of TCR clones was enriched in a specific UMAP cluster, an 'Enrichment_score' was generated based on a hypergeometric distribution, while removing potential biases caused by cell number differences from each patient. For example, from a given patient '*PT*', there were in total '*O*' cells sequenced, and for a given T cell clone, there were in total '*n*' cells belonging to this clonotype. Among these cells, there were '*m*' total cells found in *cluster A* which had '*N*'

number of cells in this cluster from '*PT*'. Then the Enrichment_score for this clonotype in $cluster\ A = \frac{m}{\frac{n}{o} \times N}$.

Bulk TCR DNA sequencing and data processing:

Both frozen and archival paraffin embedded specimens were processed for bulk TCR vβ DNA sequence analysis. Skin, tumor, and blood samples were dry frozen at −80°C, and DNA was extracted using the DNeasy Blood & Tissue Kit from QIAGEN (Cat No./ID: 69504). Archival FFPE tumors were obtained from the Pathology Department at Dartmouth-Hitchcock Medical Center. Five to ten 5mm rolls of the embedded tumor specimens were cut, and the QIAamp DNA FFPE Tissue Kit (Cat No./ID: 56404) was used to deparaffinate and extract DNA from these samples. All extracted DNA samples were cleaned for PCR inhibition factors, such as melanin, using the OneStep PCR Inhibitor Removal Kit by ZYMO RESEARCH (cat no. D6030). DNA concentration and purity were measured by Nanodrop analysis. TCR sequencing service was provided by Adaptive Biotechnologies. Briefly, 3ug or 5ug quantities of DNA were submitted for 'survey' or 'deep' resolution, respectively. Skin and non-lymphoid metastatic tumors received 'survey' resolution, whereas PBMCs and lymph node metastatic tumors received 'deep' resolution. Deep sequencing of the TCR β-chain (*TRB* gene) was performed by the immunoSEQ platform. Only data from productive rearrangements were exported from the immunoSEQ Analyzer for further analysis. For skin samples, there were on average 11,728 TCR templates (range 1715–31,251) detected, representing an average of 5116 unique clonotypes (range 1015–17,175). For tumor samples, there were on average 15,990 TCR templates (range 183–65,181) detected, representing an average of 10,849 unique clonotypes (range 147–57,341). Blood samples had on average 36,159 TCR templates (range 13,164–50,201) detected, representing an average of 21,895 unique clonotypes (range 9,237–36,253). Sequencing depth was 10–20-fold deeper than scTCR-seq.

To call matched TCR clones between different tissues, whole CDR3 nucleotide sequences for *TRB* genes required identical sequence matching. An index of shared clonality was based on a previously published method[15]. "Match_index" was defined as equaling $\frac{N}{N1 \times N2} \times 100{,}000$ with N representing the number of matched clonotypes between two tissues, and N1 and N2 denoting the total number of clonotypes in each tissue, respectively. The constant 100,000 was used to elevate the index to a readable magnitude. This method was used to exclude potential biases caused by the varying library sizes of different samples.

To identify long-persisting TCR clonotypes, clones were identified from archival tumor specimens taken at least three years prior to skin or blood collection. TCR clonotypes that were highly expanded (frequency>0.2%, leading to at least 5 cells of each clone) in these tumors were identified and matched to clones in skin and blood.

Long-persisting T-cell clones that were identified by bulk TCR-seq were compared with patient-matched TCR β-chains from scTCR-seq data. This analysis was only applicable to one patient (PT635) who had both a banked tumor from 6 years prior and an adequate number of clones in scTCR-seq data. Four clones were identified for which at least two cells

were present in the skin specimen. For these four clonotypes, cell barcodes were retrieved, and RNA-seq profiles were highlighted in a UMAP projection. Cluster enrichment indices for these clones were calculated as described above.

Statistical analysis and reproducibility:

Significance was evaluated using the following statistical analyses: two-tailed paired Student's *t-test,* one-tailed paired Student's *t-test*, one-tailed unpaired Student's *t-test*, two-sided permutation test with multiple testing correction by the BH-FDR method, two-sided long-rank test, two-sided fisher exact test and the two-sided Wald test. These analyses were performed using R (version 3.6.0) or the GSEA_4.0.3 software. $P < 0.05$ was considered statistically significant. The calculation of differentially expressed genes between different clusters in the scRNA-seq data was performed using two-sided Wilcoxon rank sum test and P-values were corrected for multiple comparisons with the Bonferroni method. No statistical method was used to predetermine sample sizes. Experiments were not randomized, and investigators were not blinded. Each patient tissue was considered an independent biological sample in the study. To focus on $CD8^+$ T cells, sorted $CD4^+$ T cells were excluded from these analyses.

Reporting Summary:

Further information on research design and reagents is available in the Nature Research Reporting Summary linked to this article.

Extended Data

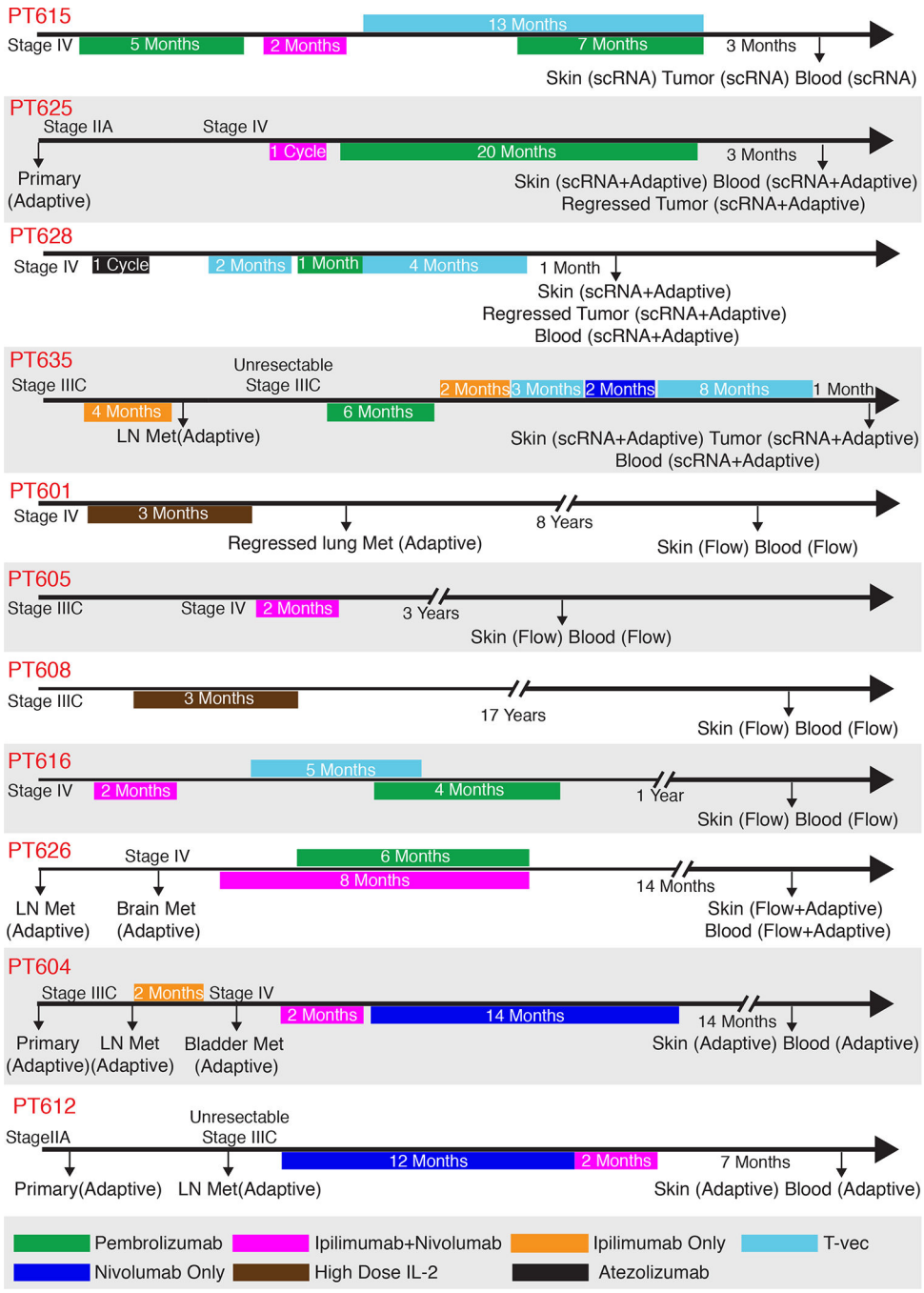

Extended Data Fig. 1. Summary of melanoma patient treatments and specimens

Detailed summary of the melanoma clinical stage, types and durations of immunotherapy treatments, and specimens collected per patient. Large arrow indicates the timeline for individual patient (not to scale). The time between date of last treatment and tissue biopsy is annotated in black. Small arrows show the timepoints of each specimen collection along with the experiments done for each specimen annotated in parentheses. scRNA=scRNA/

scTCR-seq; flow = flow cytometry; Adaptive = TCR Vb DNA sequencing. Different colors indicate different types of immunotherapy as depicted in the legend.

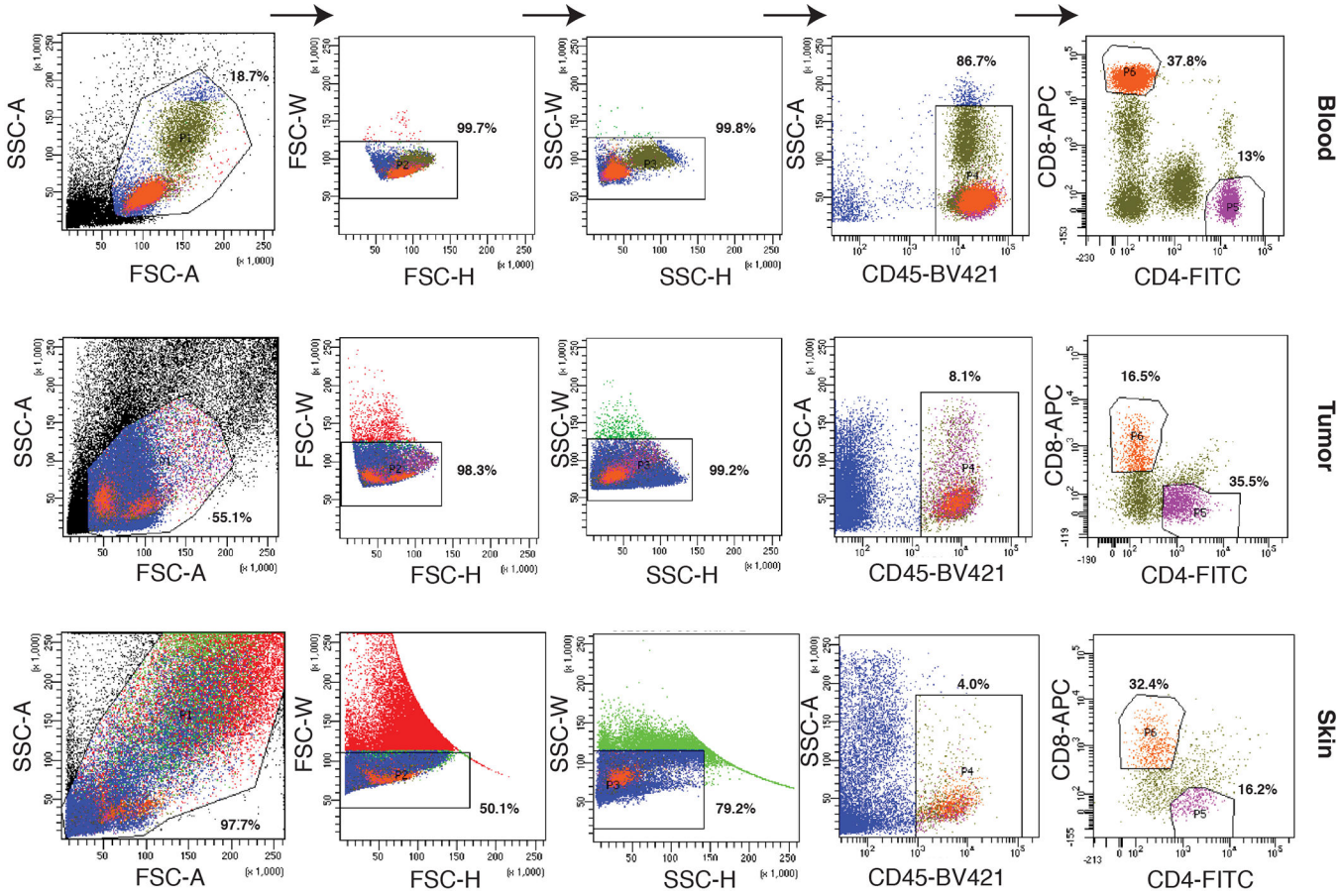

Extended Data Fig. 2. FACS gating strategy

Pseudocolor graphs show the gating strategy for FACS of each tissue. $CD45^+CD8^+$ and $CD45^+CD4^+$ cells were sorted by FACS into the same well. Values of x and y axis represent fluorescence intensities. Percentages of cell populations were labelled in each graph.

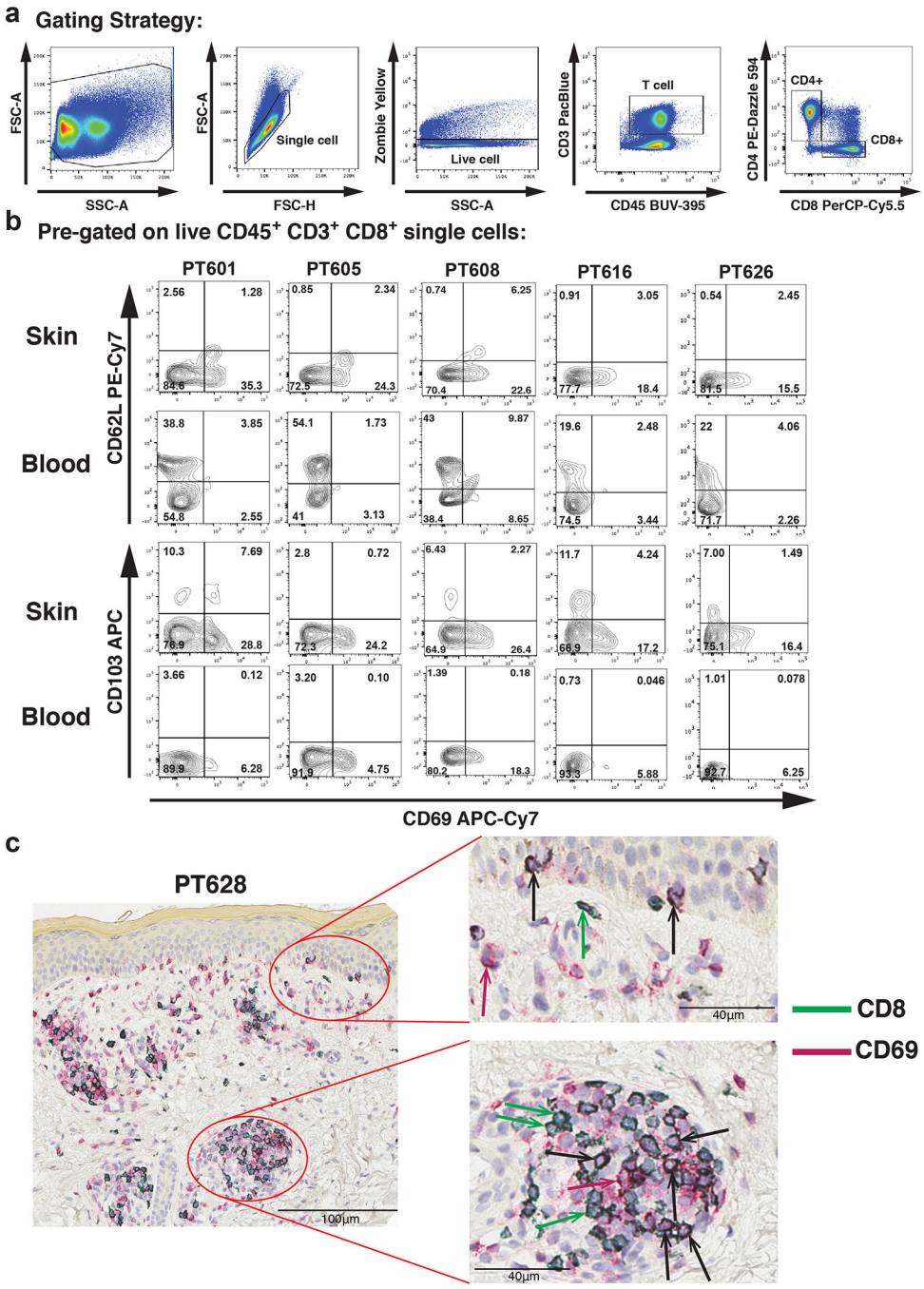

Extended Data Fig. 3. Resident memory CD8$^+$ T cells expressing CD69 reside in both the epidermis and dermis in long-term metastatic melanoma survivors with immunotherapy-associated vitiligo

(a) Representative pseudocolor dot plots showing the gating strategy for the live CD45$^+$ CD3$^+$ CD8$^+$ population. (b) Contour plots show the expression of CD69, CD103 and CD62L on pre-gated CD8$^+$ population by flow cytometry. The number represents the proportion out of total CD8$^+$ T cells. (c) Immunohistochemistry staining for CD8$^+$ CD69$^+$ resident memory CD8$^+$ T cells in the skin from patient PT628. Images are representative of multiple fields from at least three skin sections taken from each of 4 individual patients.

CD8 was stained in green and CD69 was stained in red. CD8+ and CD69+ single-stain cells are indicated by green and red arrows, respectively. Black cells (indicated by black arrows) are $CD8^{+}CD69^{+}$ co-stained cells. Original magnification: 10X (left) and 40X (right).

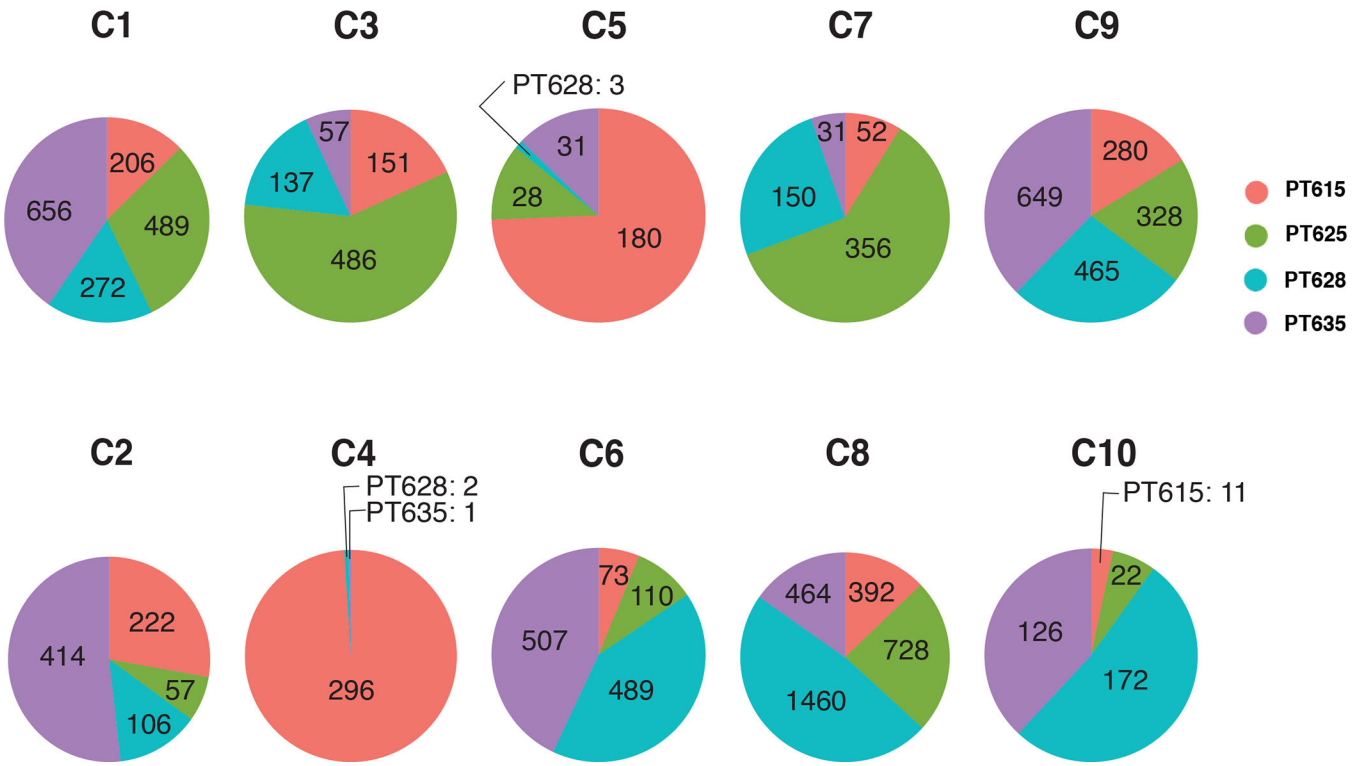

Extended Data Fig. 4. Patient contributions to each $CD8^{+}$ T-cell cluster

Pie charts depicting the proportion of cells from each patient to the total number of cells in each cluster (C1-C10). Each color represents one individual patient, with the absolute number of cells from each patient labeled in the corresponding slice of the pie chart.

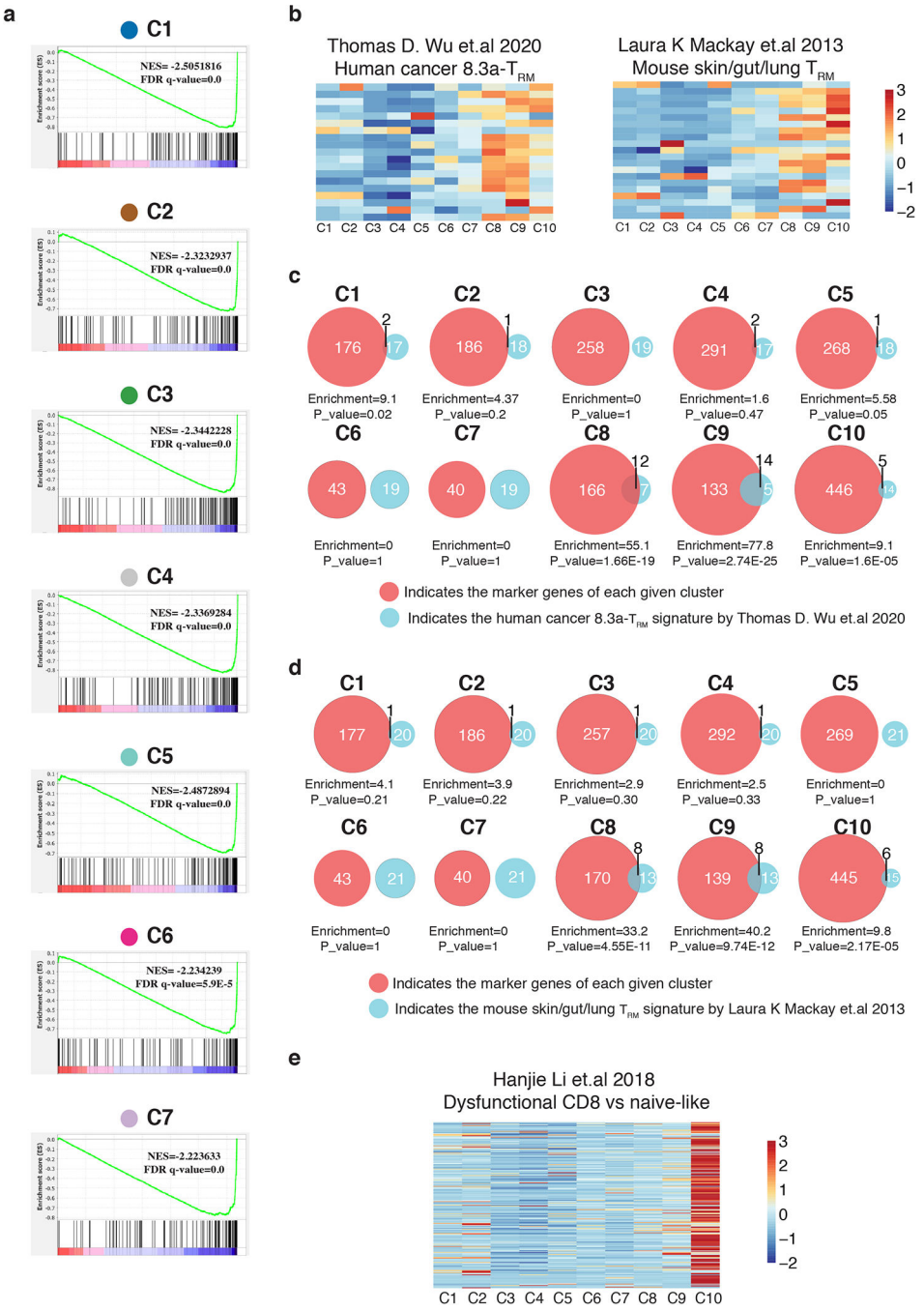

Extended Data Fig. 5. Transcriptional profiles of clusters C8-C10 are enriched in consensus T_{RM} gene lists while the transcription profiles of clusters C1-C7 are not enriched for core T_{RM} genes

(a) GSEA analysis showing that the upregulated genes of T_{RM} were enriched in the downregulated genes in clusters C1-C7 demonstrating that only clusters C8-C10 have key features of T_{RM}. NESs and FDR q-values are shown for each gene set. The statistics were performed by the two-sample Kolmogorov-Smirnov test. (b) Heatmaps depict the z-transformed mean expression of published consensus skin or tumor T_{RM} gene lists across $CD8^+$ T cell clusters C1-C10. (c) Venn diagrams show the number of genes that overlap between the marker gene list of each cluster (red circle) with the published human cancer

T_{RM} gene list (blue circle). The overlap levels between two gene lists were evaluated by two-sided fisher exact test. Enrichment scores and P-values are labeled accordingly. (d)Venn diagrams show the number of genes that overlap between the marker gene list of each cluster (red circle) with the published mouse skin/gut/lung T_{RM} gene list (blue circle). The overlap levels between two gene lists were evaluated by two-sided fisher exact test. Enrichment scores and P-values are labeled accordingly. (e) Heatmap depicts the z-transformed mean expression of a published melanoma infiltrating dysfunctional $CD8^+$ gene list across clusters C1-C10.

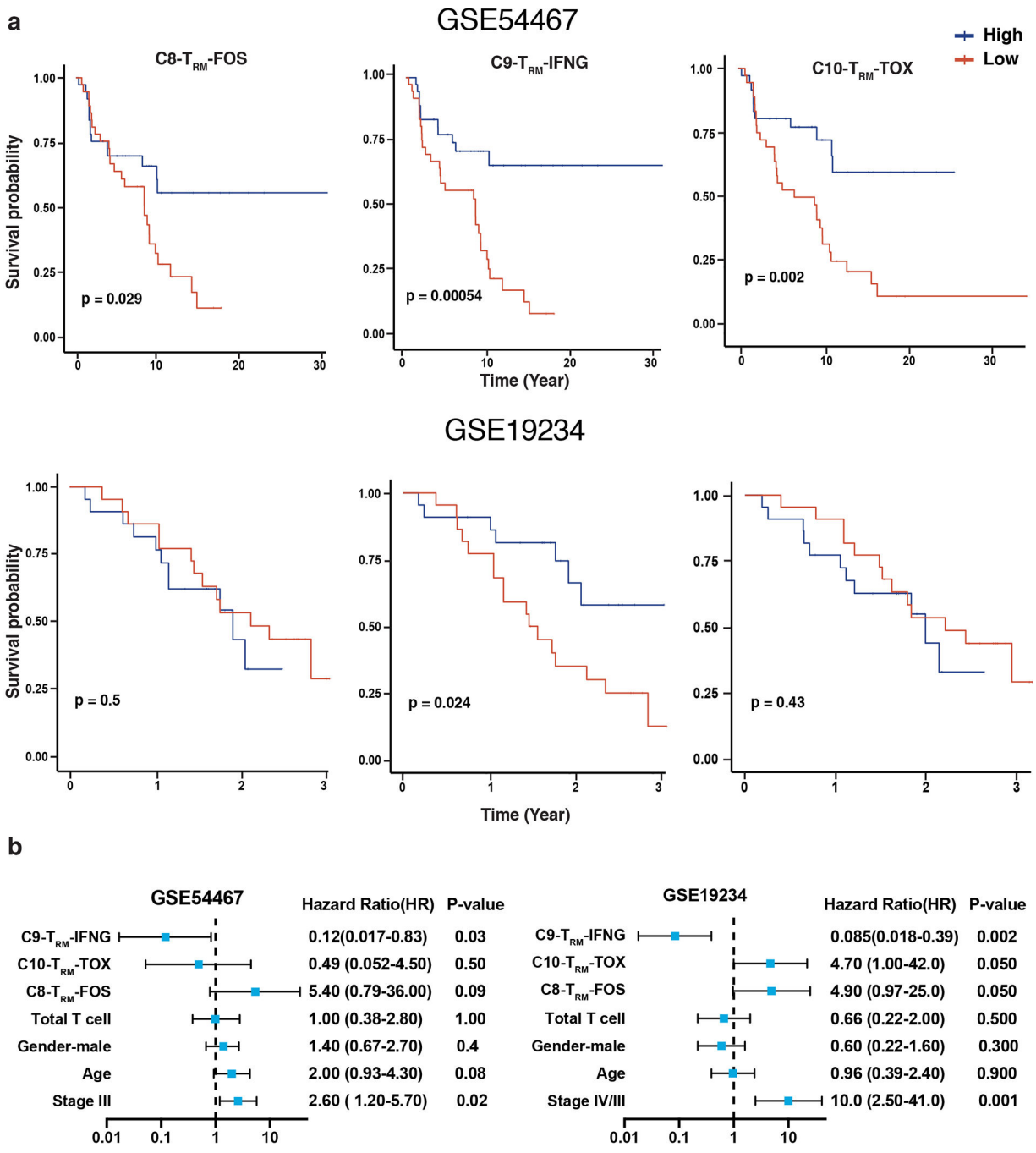

Extended Data Fig. 6. T_{RM}-IFNG signature is superior in predicting the survival of stage III/IV melanoma patients

(a) Kaplan–Meier overall survival curves of melanoma patients from two different published datasets, GSE54467 (top, n=75 patients) and GSE19324 (bottom, n=44 patients), stratified by enrichment of signatures derived from each of three TRM clusters. High and low groups were separated by the median value of the Z-transformed normalized mean expression of each gene set (top: N= 37 patients high and N=38 patients low; bottom: N=22 patients high and N=22 patients low). P-values were calculated by two-sided log-rank test. OR P-values were calculated by multivariate Cox regression. (b) Multivariable cox survival regression

model evaluating the individual contribution of different variables to the prognosis of melanoma patients from the above datasets, GSE54467 (left) and GSE19324 (right). Forest plots show the means of hazard ratios (HRs) represented by blue squares, the 95% confidence intervals of HRs represented by horizontal bars, and p-values calculated by the two-sided Wald test for each variable.

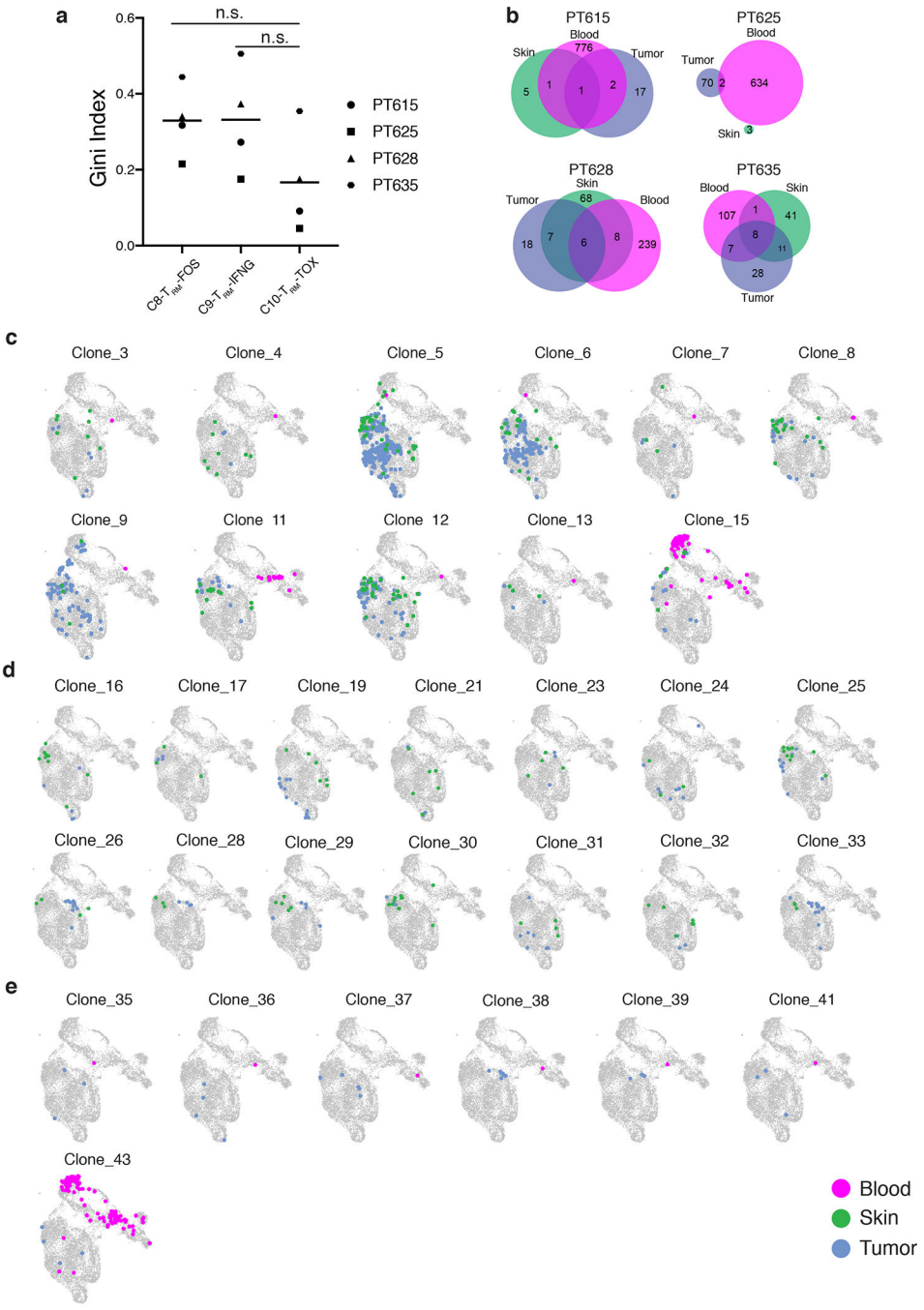

Extended Data Fig. 7. Tumor-associated TCR clonotypes in the skin and blood of long-term metastatic melanoma survivors

(a) Gini indexes of each tissue (left) or each T_{RM} cluster (right) calculated for n=4 individual patients, showing no significant differences in baseline clonal expansion among different tissues or different T_{RM} clusters. The lines indicate the average Gini index across all four patients for each cluster. Two-sided Wilcoxon test. (b) Venn diagrams showing the number of matched TCR clonotypes between different specimens from individual patients. Colors indicate different tissue origins. The number of TCR clonotypes belonging to each group was labeled accordingly. (c) The distribution of the remaining Resident/Circulating clonotypes (11/15) to the UMAP plot. Dots indicate $CD8^+$ T cells from the same clone. Colors designate different specimen types. (d) The distribution of the remaining Resident-Only clonotypes (14/18) to the UMAP plot. Dots indicate $CD8^+$ T cells from the same clone. Colors designate different specimen types. (e) The distribution of the remaining Circulation-Capable clonotypes (7/11) to the UMAP plot. Dots indicate $CD8^+$ T cells from the same clone. Colors designate different specimen types.

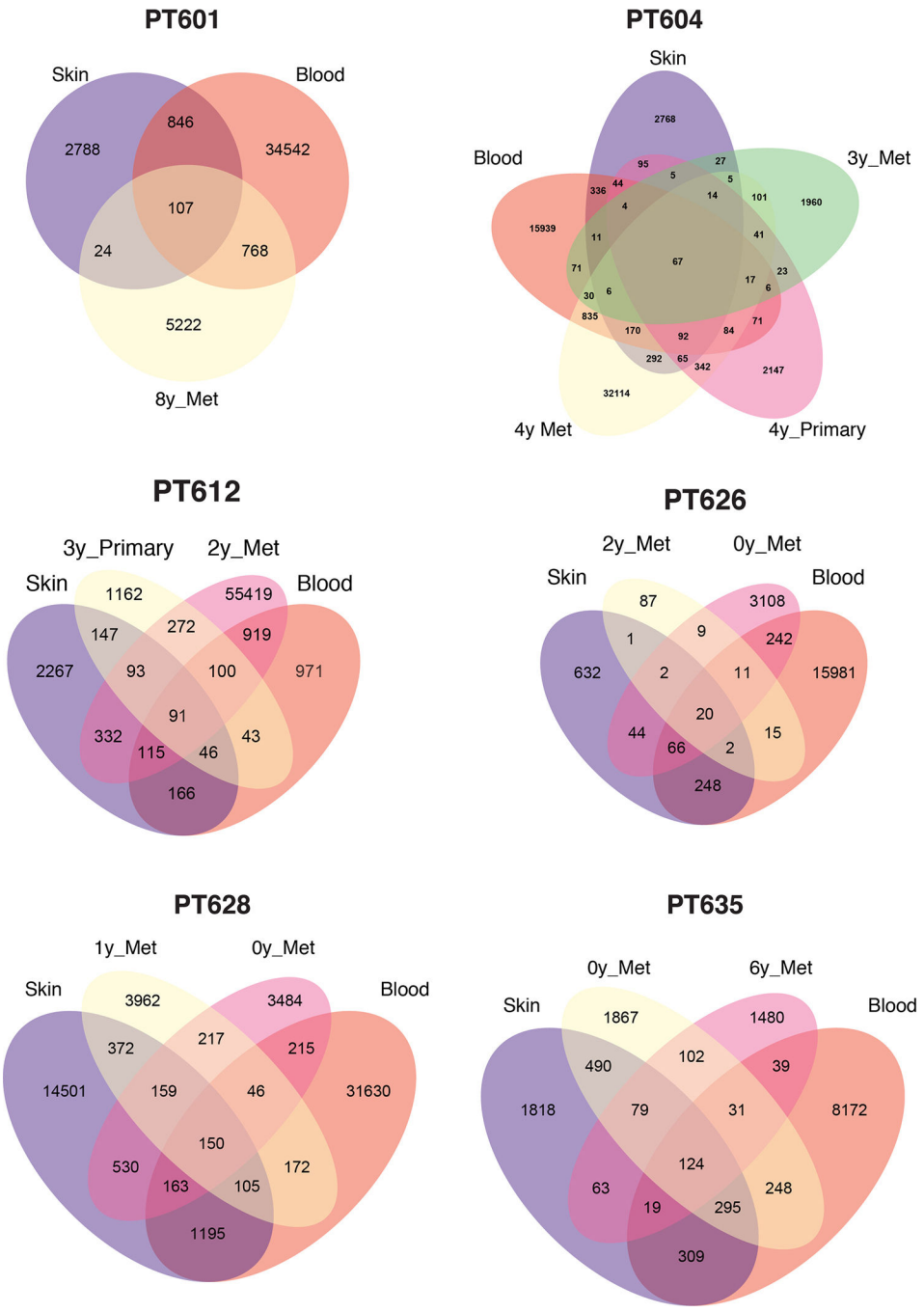

Extended Data Fig. 8. Tumor-associated clonotypes in the skin and blood of patients

Venn diagrams showing the number of matched TCR clonotypes between skin, blood and historically banked tumors of each patient. The number of TCR clonotypes belonging to each group was labeled accordingly.

Supplementary Material

Refer to Web version on PubMed Central for supplementary material.

Acknowledgments

We are truly grateful for the generosity of all the patients who volunteered their time and tissue for this study. We thank the nursing staff of the General Surgery clinic at Dartmouth-Hitchcock Medical Center led by L. O'Rourke, and the Norris Cotton Cancer Center melanoma research team, especially B. Highhouse and M. Stannard, for assistance in patient recruitment and coordination. We appreciate the effort from the core facilities - the Dartlab and the Single Cell Genomics Core - at Dartmouth. We thank Gary Ward at the Dartlab for FACS sorting expertise. We thank M. Pasca di Magliano for discussion and advice. This work was funded by The Dartmouth CTSA (NIH KL2TR0010), the American Cancer Society (CSDG 18–167-01), the Dow-Crichlow Career Development Award in Surgery, and the Society of Surgical Oncology Clinical Investigator Award, to CVA.; NIH R01 CA225028 and The Knights of the York Cross of Honour Philanthropic Fund to MJT; a Borroughs Welcome BDLS Training Grant to JH; NIH F31CA232554 to AM, and support from 5P30 CA023108–40 (Immune Monitoring and Genomics and Molecular Biology Shared Resources). Single cell sequencing was conducted at the Dartmouth Center for Quantitative Biology with support from NIGMS (P20GM130454) and NIH S10 (S10OD025235) awards. The views expressed are those of the authors and not necessarily those of the NIH or the American Cancer Society.

References

1. Larkin J et al. Five-Year Survival with Combined Nivolumab and Ipilimumab in Advanced Melanoma. N Engl J Med 381, 1535–1546, doi:10.1056/NEJMoa1910836 (2019). [PubMed: 31562797]
2. Robert C et al. Nivolumab in previously untreated melanoma without BRAF mutation. N Engl J Med 372, 320–330, doi:10.1056/NEJMoa1412082 (2015). [PubMed: 25399552]
3. Weber JS et al. Nivolumab versus chemotherapy in patients with advanced melanoma who progressed after anti-CTLA-4 treatment (CheckMate 037): a randomised, controlled, open-label, phase 3 trial. Lancet Oncol 16, 375–384, doi:10.1016/S1470-2045(15)70076-8 (2015). [PubMed: 25795410]
4. Huang AC et al. T-cell invigoration to tumour burden ratio associated with anti-PD-1 response. Nature 545, 60–65, doi:10.1038/nature22079 (2017). [PubMed: 28397821]
5. Krieg C et al. High-dimensional single-cell analysis predicts response to anti-PD-1 immunotherapy. Nat Med 24, 144–153, doi:10.1038/nm.4466 (2018). [PubMed: 29309059]
6. Ribas A et al. PD-1 Blockade Expands Intratumoral Memory T Cells. Cancer Immunol Res 4, 194–203, doi:10.1158/2326-6066.CIR-15-0210 (2016). [PubMed: 26787823]
7. Sade-Feldman M et al. Defining T Cell States Associated with Response to Checkpoint Immunotherapy in Melanoma. Cell 175, 998–1013 e1020, doi:10.1016/j.cell.2018.10.038 (2018). [PubMed: 30388456]
8. Freeman-Keller M et al. Nivolumab in Resected and Unresectable Metastatic Melanoma: Characteristics of Immune-Related Adverse Events and Association with Outcomes. Clin Cancer Res 22, 886–894, doi:10.1158/1078-0432.CCR-15-1136 (2016). [PubMed: 26446948]
9. Hua C et al. Association of Vitiligo With Tumor Response in Patients With Metastatic Melanoma Treated With Pembrolizumab. JAMA Dermatol 152, 45–51, doi:10.1001/jamadermatol.2015.2707 (2016). [PubMed: 26501224]
10. Nakamura Y et al. Correlation between vitiligo occurrence and clinical benefit in advanced melanoma patients treated with nivolumab: A multi-institutional retrospective study. J Dermatol 44, 117–122, doi:10.1111/1346-8138.13520 (2017). [PubMed: 27510892]
11. Malik BT et al. Resident memory T cells in the skin mediate durable immunity to melanoma. Sci Immunol 2, doi:10.1126/sciimmunol.aam6346 (2017).
12. Gerlach C et al. The Chemokine Receptor CX3CR1 Defines Three Antigen-Experienced CD8 T Cell Subsets with Distinct Roles in Immune Surveillance and Homeostasis. Immunity 45, 1270–1284, doi:10.1016/j.immuni.2016.10.018 (2016). [PubMed: 27939671]
13. Sallusto F, Lenig D, Forster R, Lipp M & Lanzavecchia A Two subsets of memory T lymphocytes with distinct homing potentials and effector functions. Nature 401, 708–712, doi:10.1038/44385 (1999). [PubMed: 10537110]
14. Herndler-Brandstetter D et al. KLRG1(+) Effector CD8(+) T Cells Lose KLRG1, Differentiate into All Memory T Cell Lineages, and Convey Enhanced Protective Immunity. Immunity 48, 716–729 e718, doi:10.1016/j.immuni.2018.03.015 (2018). [PubMed: 29625895]

15. Guo X et al. Global characterization of T cells in non-small-cell lung cancer by single-cell sequencing. Nat Med 24, 978–985, doi:10.1038/s41591-018-0045-3 (2018). [PubMed: 29942094]
16. Martin MD & Badovinac VP Defining Memory CD8 T Cell. Front Immunol 9, 2692, doi:10.3389/fimmu.2018.02692 (2018). [PubMed: 30515169]
17. Muri J et al. The thioredoxin-1 system is essential for fueling DNA synthesis during T-cell metabolic reprogramming and proliferation. Nat Commun 9, 1851, doi:10.1038/s41467-018-04274-w (2018). [PubMed: 29749372]
18. Wei H et al. Cutting Edge: Foxp1 Controls Naive CD8+ T Cell Quiescence by Simultaneously Repressing Key Pathways in Cellular Metabolism and Cell Cycle Progression. J Immunol 196, 3537–3541, doi:10.4049/jimmunol.1501896 (2016). [PubMed: 27001958]
19. Zheng C et al. Landscape of Infiltrating T Cells in Liver Cancer Revealed by Single-Cell Sequencing. Cell 169, 1342–1356 e1316, doi:10.1016/j.cell.2017.05.035 (2017). [PubMed: 28622514]
20. Szabo PA et al. Single-cell transcriptomics of human T cells reveals tissue and activation signatures in health and disease. Nat Commun 10, 4706, doi:10.1038/s41467-019-12464-3 (2019). [PubMed: 31624246]
21. Hurton LV et al. Tethered IL-15 augments antitumor activity and promotes a stem-cell memory subset in tumor-specific T cells. Proc Natl Acad Sci U S A 113, E7788–E7797, doi:10.1073/pnas.1610544113 (2016). [PubMed: 27849617]
22. Gattinoni L et al. A human memory T cell subset with stem cell-like properties. Nat Med 17, 1290–1297, doi:10.1038/nm.2446 (2011). [PubMed: 21926977]
23. Molodtsov A & Turk MJ Tissue Resident CD8 Memory T Cell Responses in Cancer and Autoimmunity. Front Immunol 9, 2810, doi:10.3389/fimmu.2018.02810 (2018). [PubMed: 30555481]
24. Kumar BV et al. Human Tissue-Resident Memory T Cells Are Defined by Core Transcriptional and Functional Signatures in Lymphoid and Mucosal Sites. Cell Rep 20, 2921–2934, doi:10.1016/j.celrep.2017.08.078 (2017). [PubMed: 28930685]
25. Wu TD et al. Peripheral T cell expansion predicts tumour infiltration and clinical response. Nature 579, 274–278, doi:10.1038/s41586-020-2056-8 (2020). [PubMed: 32103181]
26. Mackay LK et al. The developmental pathway for CD103(+)CD8+ tissue-resident memory T cells of skin. Nat Immunol 14, 1294–1301, doi:10.1038/ni.2744 (2013). [PubMed: 24162776]
27. Cheuk S et al. CD49a Expression Defines Tissue-Resident CD8(+) T Cells Poised for Cytotoxic Function in Human Skin. Immunity 46, 287–300, doi:10.1016/j.immuni.2017.01.009 (2017). [PubMed: 28214226]
28. Li H et al. Dysfunctional CD8 T Cells Form a Proliferative, Dynamically Regulated Compartment within Human Melanoma. Cell 176, 775–789 e718, doi:10.1016/j.cell.2018.11.043 (2019). [PubMed: 30595452]
29. Savas P et al. Single-cell profiling of breast cancer T cells reveals a tissue-resident memory subset associated with improved prognosis. Nat Med 24, 986–993, doi:10.1038/s41591-018-0078-7 (2018). [PubMed: 29942092]
30. Pasetto A et al. Tumor- and Neoantigen-Reactive T-cell Receptors Can Be Identified Based on Their Frequency in Fresh Tumor. Cancer Immunol Res 4, 734–743, doi:10.1158/2326-6066.CIR-16-0001 (2016). [PubMed: 27354337]
31. Fairfax BP et al. Peripheral CD8(+) T cell characteristics associated with durable responses to immune checkpoint blockade in patients with metastatic melanoma. Nat Med 26, 193–199, doi:10.1038/s41591-019-0734-6 (2020). [PubMed: 32042196]
32. Haymaker CL et al. Metastatic Melanoma Patient Had a Complete Response with Clonal Expansion after Whole Brain Radiation and PD-1 Blockade. Cancer Immunol Res 5, 100–105, doi:10.1158/2326-6066.CIR-16-0223 (2017). [PubMed: 28062513]
33. Tarhini A et al. Neoadjuvant ipilimumab (3 mg/kg or 10 mg/kg) and high dose IFN-alpha2b in locally/regionally advanced melanoma: safety, efficacy and impact on T-cell repertoire. J Immunother Cancer 6, 112, doi:10.1186/s40425-018-0428-5 (2018). [PubMed: 30352626]
34. Edwards J et al. CD103(+) Tumor-Resident CD8(+) T Cells Are Associated with Improved Survival in Immunotherapy-Naive Melanoma Patients and Expand Significantly During Anti-PD-1

Treatment. Clin Cancer Res 24, 3036–3045, doi:10.1158/1078-0432.CCR-17-2257 (2018). [PubMed: 29599411]

35. Park SL et al. Tissue-resident memory CD8(+) T cells promote melanoma-immune equilibrium in skin. Nature 565, 366–371, doi:10.1038/s41586-018-0812-9 (2019). [PubMed: 30598548]
36. Shankaran V et al. IFNgamma and lymphocytes prevent primary tumour development and shape tumour immunogenicity. Nature 410, 1107–1111, doi:10.1038/35074122 (2001). [PubMed: 11323675]
37. Higgs BW et al. Interferon Gamma Messenger RNA Signature in Tumor Biopsies Predicts Outcomes in Patients with Non-Small Cell Lung Carcinoma or Urothelial Cancer Treated with Durvalumab. Clin Cancer Res 24, 3857–3866, doi:10.1158/1078-0432.CCR-17-3451 (2018). [PubMed: 29716923]
38. Karachaliou N et al. Interferon gamma, an important marker of response to immune checkpoint blockade in non-small cell lung cancer and melanoma patients. Ther Adv Med Oncol 10, 1758834017749748, doi:10.1177/1758834017749748 (2018). [PubMed: 29383037]
39. Alspach E, Lussier DM & Schreiber RD Interferon gamma and Its Important Roles in Promoting and Inhibiting Spontaneous and Therapeutic Cancer Immunity. Cold Spring Harb Perspect Biol 11, doi:10.1101/cshperspect.a028480 (2019).
40. Gaide O et al. Common clonal origin of central and resident memory T cells following skin immunization. Nat Med 21, 647–653, doi:10.1038/nm.3860 (2015). [PubMed: 25962122]
41. Slutter B et al. Dynamics of influenza-induced lung-resident memory T cells underlie waning heterosubtypic immunity. Sci Immunol 2, doi:10.1126/sciimmunol.aag2031 (2017).
42. Fonseca R et al. Developmental plasticity allows outside-in immune responses by resident memory T cells. Nat Immunol 21, 412–421, doi:10.1038/s41590-020-0607-7 (2020). [PubMed: 32066954]
43. Jiang T et al. Tumor neoantigens: from basic research to clinical applications. J Hematol Oncol 12, 93, doi:10.1186/s13045-019-0787-5 (2019). [PubMed: 31492199]
44. Schumacher TN & Schreiber RD Neoantigens in cancer immunotherapy. Science 348, 69–74, doi:10.1126/science.aaa4971 (2015). [PubMed: 25838375]
45. Butler A, Hoffman P, Smibert P, Papalexi E & Satija R Integrating single-cell transcriptomic data across different conditions, technologies, and species. Nat Biotechnol 36, 411–420, doi:10.1038/nbt.4096 (2018). [PubMed: 29608179]
46. Stuart T et al. Comprehensive Integration of Single-Cell Data. Cell 177, 1888–1902 e1821, doi:10.1016/j.cell.2019.05.031 (2019). [PubMed: 31178118]
47. Hafemeister C & Satija R Normalization and variance stabilization of single-cell RNA-seq data using regularized negative binomial regression. Genome Biol 20, 296, doi:10.1186/s13059-019-1874-1 (2019). [PubMed: 31870423]
48. Elpek KG et al. The tumor microenvironment shapes lineage, transcriptional, and functional diversity of infiltrating myeloid cells. Cancer Immunol Res 2, 655–667, doi:10.1158/2326-6066.CIR-13-0209 (2014). [PubMed: 24801837]
49. Painter MW et al. Transcriptomes of the B and T lineages compared by multiplatform microarray profiling. J Immunol 186, 3047–3057, doi:10.4049/jimmunol.1002695 (2011). [PubMed: 21307297]
50. Bolstad BM, Irizarry RA, Astrand M & Speed TP A comparison of normalization methods for high density oligonucleotide array data based on variance and bias. Bioinformatics 19, 185–193, doi:10.1093/bioinformatics/19.2.185 (2003). [PubMed: 12538238]
51. Leek JT, Johnson WE, Parker HS, Jaffe AE & Storey JD The sva package for removing batch effects and other unwanted variation in high-throughput experiments. Bioinformatics 28, 882–883, doi:10.1093/bioinformatics/bts034 (2012). [PubMed: 22257669]
52. Varn FS, Wang Y, Mullins DW, Fiering S & Cheng C Systematic Pan-Cancer Analysis Reveals Immune Cell Interactions in the Tumor Microenvironment. Cancer Res 77, 1271–1282, doi:10.1158/0008-5472.CAN-16-2490 (2017). [PubMed: 28126714]
53. Liberzon A et al. The Molecular Signatures Database (MSigDB) hallmark gene set collection. Cell Syst 1, 417–425, doi:10.1016/j.cels.2015.12.004 (2015). [PubMed: 26771021]

54. Subramanian A et al. Gene set enrichment analysis: a knowledge-based approach for interpreting genome-wide expression profiles. Proc Natl Acad Sci U S A 102, 15545–15550, doi:10.1073/pnas.0506580102 (2005). [PubMed: 16199517]

55. Zhao Y et al. A Leukocyte Infiltration Score Defined by a Gene Signature Predicts Melanoma Patient Prognosis. Mol Cancer Res 17, 109–119, doi:10.1158/1541-7786.MCR-18-0173 (2019). [PubMed: 30171176]

56. Menares E et al. Tissue-resident memory CD8(+) T cells amplify anti-tumor immunity by triggering antigen spreading through dendritic cells. Nat Commun 10, 4401, doi:10.1038/s41467-019-12319-x (2019). [PubMed: 31562311]

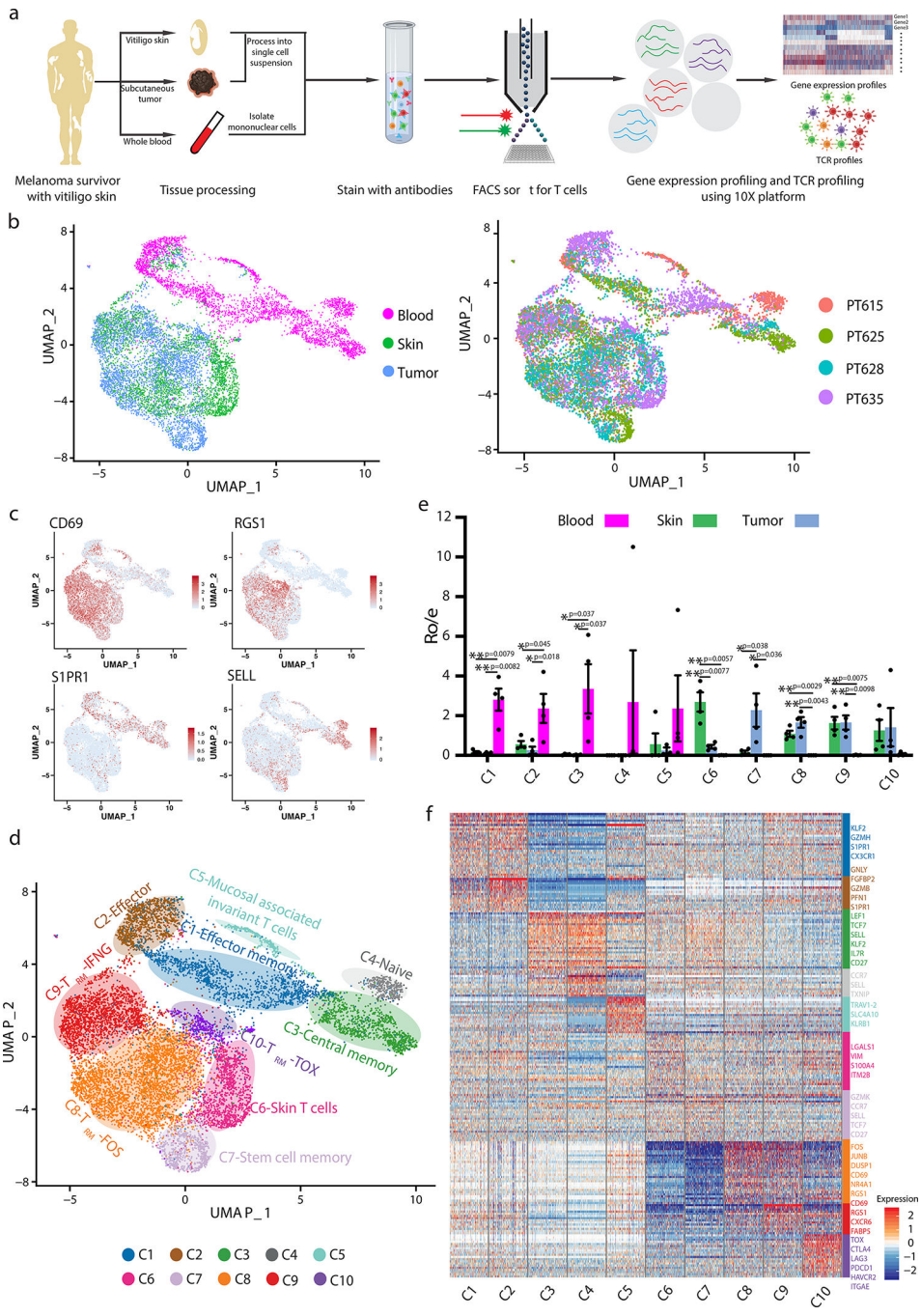

Figure 1: Overlapping transcriptional signatures of CD8$^+$ T cells from skin and tumor of long-term melanoma survivors.

(**a**) Workflow schematic. Single-cell RNA and TCR sequencing were performed on T cells sorted from vitiligo-affected skin, tumor and peripheral blood. (**b**) UMAP projection of CD8$^+$ T cells from skin, tumor and blood of four patients. Each dot corresponds to one single cell colored according to tissue (left) or patient identity (right). (**c**) Feature plots demonstrating the expression of marker genes for CD8$^+$ T-cell residency (*CD69, RGS1*) or recirculation (*S1PR1, SELL*). Color scale represents normalized gene expression level. (**d**)

UMAP projection of 10,658 $CD8^+$ T cells from skin, tumor, and blood of four patients, forming ten distinct clusters designated C1-C10 (colored as shown in the legend), with cluster names assigned based on inferred function. (**e**) Attribution of each specimen type to each cluster. The ratio between observed cell number and random expected cell number calculated by chi-square test (Ro/e) was used to evaluate enrichment, with Ro/e>1 indicating enrichment; colors indicate specimen types; black dots represent individual patients. Bars depict means with error bars representing s.e.m. for n=4 patients; $*P< 0.05$; $**P< 0.01$, by one-sided paired Student's t-test. (**f**) Heatmap of differentially expressed genes (rows) in cells from different clusters (columns) of four patients. Heatmap colors indicate z-transformed expression of genes in each row, with scale depicted in legend. Annotations (right) highlight representative genes with high differential gene expression within each cluster, relative to other clusters. Colors of gene names indicate corresponding clusters in panel d.

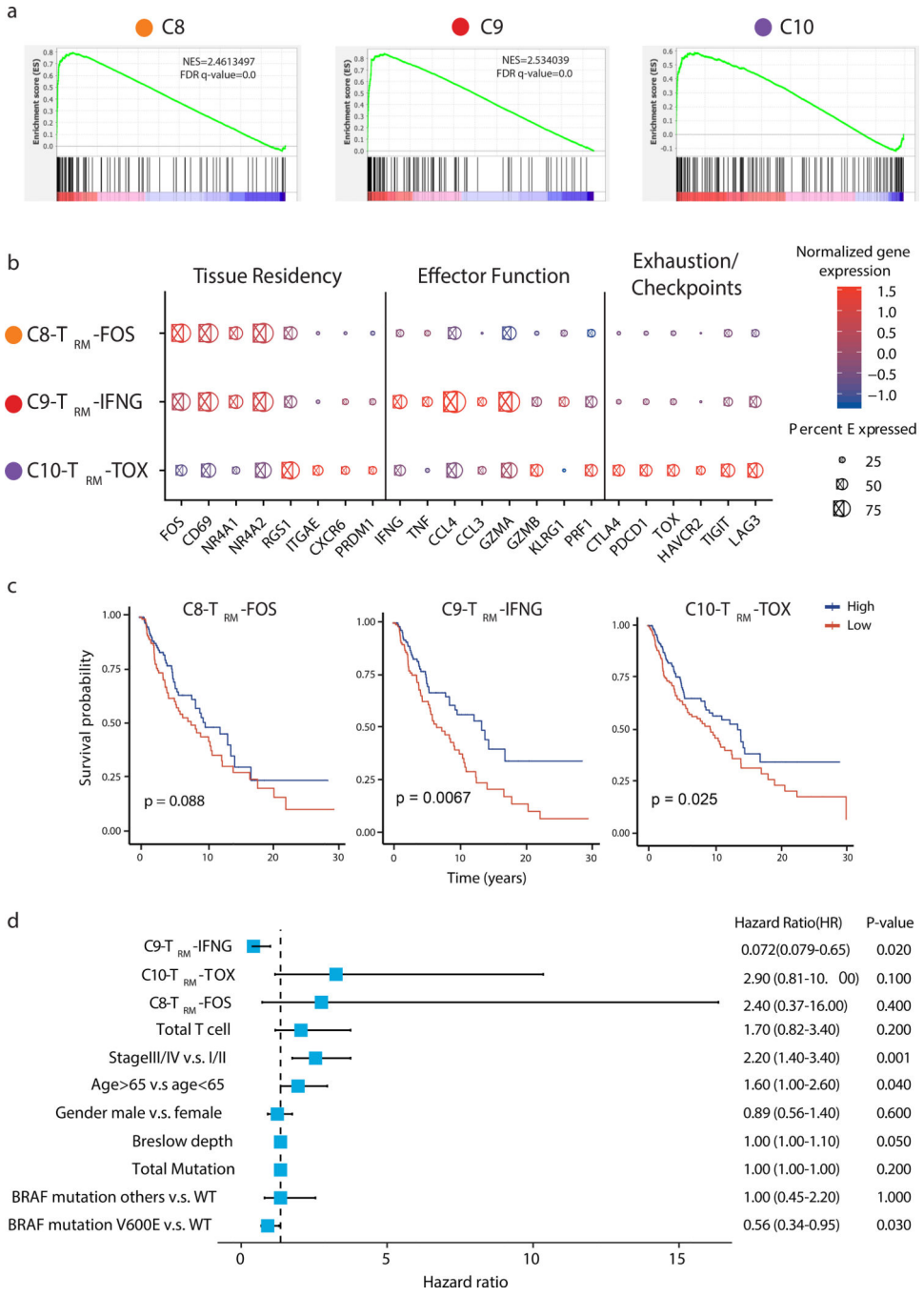

Figure 2: T_{RM} cells in skin and tumor are comprised of three subpopulations with discrete features and prognostic signatures.

(**a**) Gene Set Enrichment Analysis (GSEA) indicating that the upregulated genes of clusters C8, C9 and C10 are significantly enriched in T_{RM} markers. Ticks below the line correspond to gene ranks. Statistical analysis was performed using a two-sided permutation test with multiple testing correction by the BH-FDR method. Normalized enrichment scores (NESs) and FDR q-values are shown for each cluster. **(b)** Dot plot showing the average Z-transformed normalized expression of tissue residency, effector function and exhaustion/

checkpoint-associated genes between the three T_{RM} clusters. Size of each dot indicates the fraction of cells expressing each gene; color scale represents Z-transformed normalized expression. C8-T_{RM}-FOS, C9-T_{RM}-IFNG, and C10-T_{RM}-TOX clusters were named based on noted differentially expressed genes. **(c)** Kaplan–Meier overall survival curves of TCGA metastatic skin cutaneous melanoma (SKCM) patients stratified by enrichment of signatures derived from each of three T_{RM} clusters. High (N = 179 patients) and low (N = 177 patients) were separated by the median value of the Z-transformed normalized mean expression of each gene set. *P* values were calculated by two-sided log-rank test. **(d)** Multivariable cox survival regression model evaluating the individual contribution of different variables to the prognosis of TCGA-advanced SKCM patients. N=206 metastatic melanoma patients with all the information for the clinical variables analyzed from the TCGA dataset were applied in this analysis. Forest plot shows the means of hazard ratios (HRs) represented by blue squares, 95% confidence intervals of the HRs represented by horizontal bars, and *P* values calculated by the two-sided Wald test for each variable.

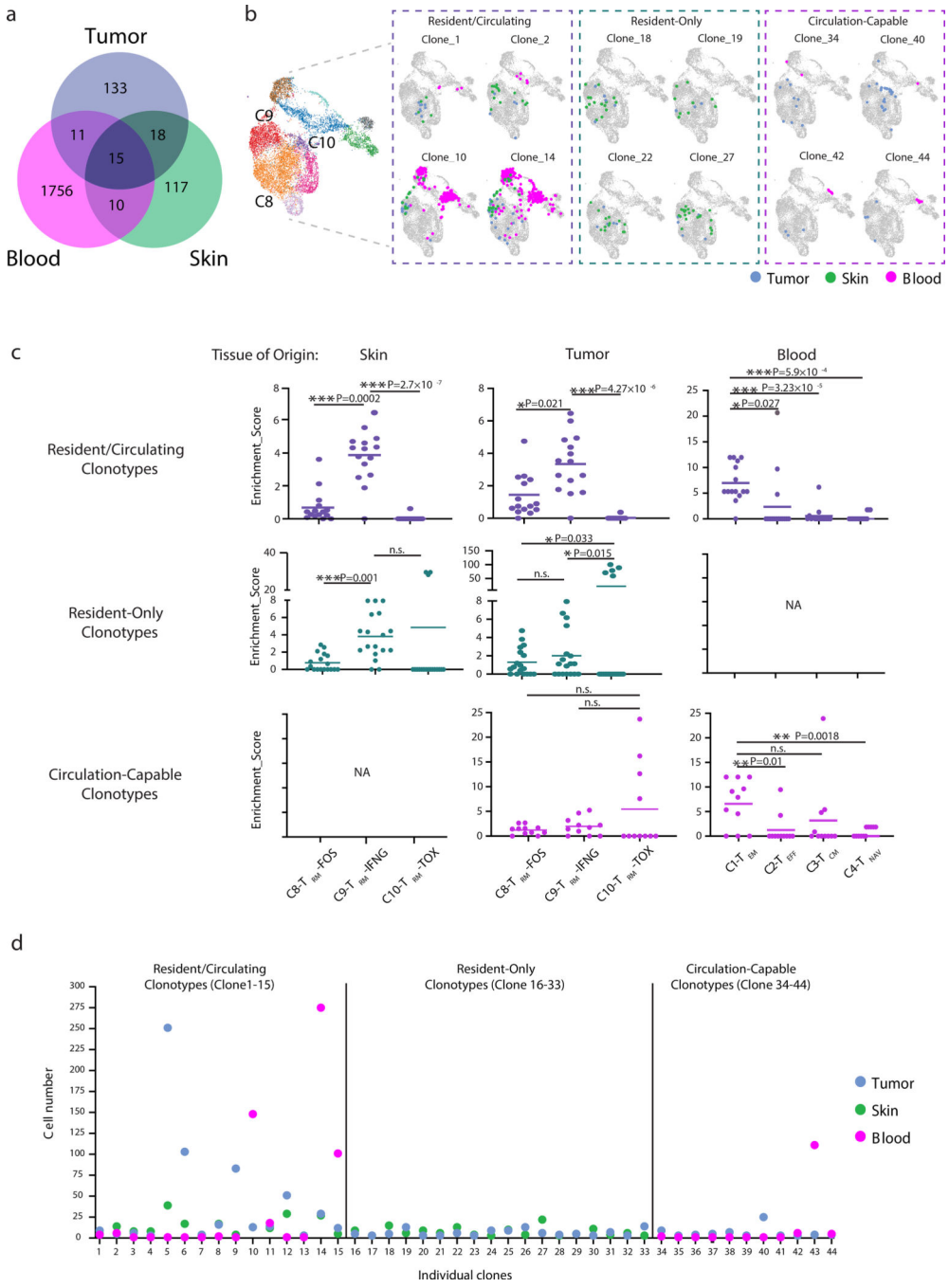

Figure 3: Promiscuously distributed CD8$^+$ T cell clonotypes show a propensity to form T_{RM}-IFNG cells in skin and tumor.

(a) Venn diagram indicating the number of shared vs. discrete TCR clonotypes (meeting defined criteria, see Methods) between different tissues in four patients. (**b**) UMAP plots indicating features of three tumor-associated clonotypic categories. Four representative clonotypes are depicted for each category. Clusters from Fig. 1d are shown for reference (left); dots represent individual cells of a given clonotype, with colors denoting T-cell tissue of origin. **(c)** Distribution of T cells from different tumor-associated clonotypic categories

among transcriptional clusters. N=15, N=18 and N=11 TCR clonotypes were analyzed for the Resident/Circulating, Resident-Only or Circulation-Capable categories respectively. X-axis indicates cluster and Y-axis depicts the Enrichment_Score (see Methods). Each dot represents a different TCR clonotype and is colored according to the category as in (a). Lines indicate average enrichment scores. NA indicates data not applicable. *$P < 0.05$; **$P < 0.01$; ***$P < 0.001$; two-sided paired Student's t-test. **(d)** Dot plot showing the clonal frequency of the 15 Resident/Circulating, 18 Resident-Only, and 11 Circulation-Capable tumor-associated TCR clonotypes in each specimen type. Colors designate different specimen types.

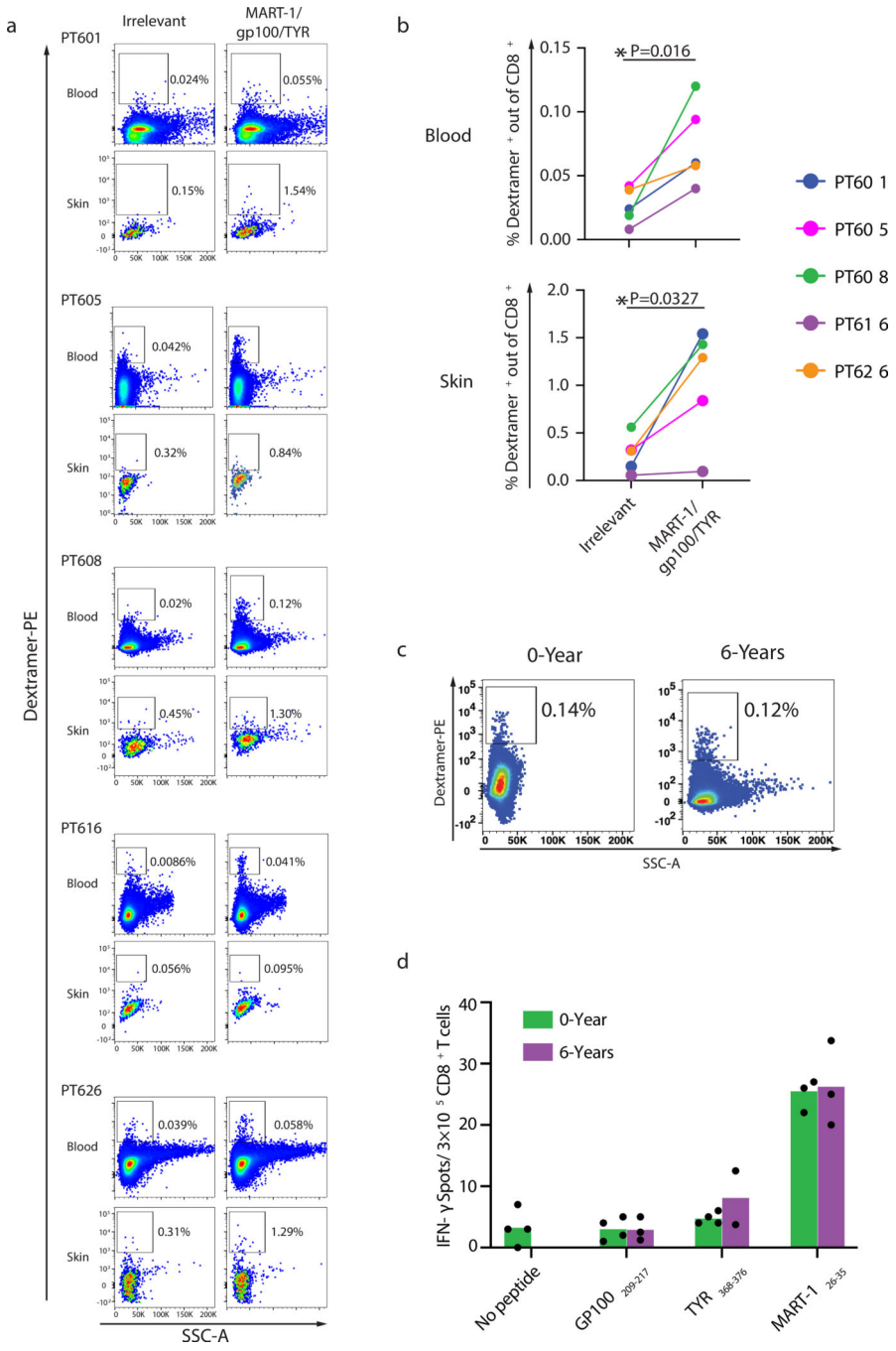

Figure 4: Melanoma antigen-specific T cells accumulate in skin and blood and are capable of long-lived functional recall.

(a) Dextramer staining of $CD8^+$ T cells specific for MART-1, gp100, and TYR dextramers (pooled) vs. irrelevant dextramer, in blood and skin. All dot plots were pre-gated on $CD45^+$ $CD3^+$ $CD8^+$ cells. Percentages represent the proportion of dextramer positive cells out of total CD8+ T cells. Data from five individual patients are shown. **(b)** Summary of % $dextramer^+$ cells out of total $CD8^+$ T cells for the 5 patients shown in panel a. Colors represent individual patients; $*P < 0.05$ by one-sided paired Student's t-test for irrelevant vs.

relevant dextramer staining. **(c)** Persistence of MART-1, gp100, and TYR (pooled)-specific response in the blood of PT608 over a period of 6 years; pre-gated on the $CD45^+$ $CD3^+$ $CD8^+$ population. **(d)** IFNγ ELISpot showing individual peptide-specific $CD8^+$ T cells in blood specimens taken from the same patient six years apart. Y-axis shows the number of IFNγ spots per 3×10^5 $CD8^+$ T cells. Dots indicate individual assay replicates (individual wells) from the same blood specimen; bars depict means. ELISpot was performed twice with similar results.

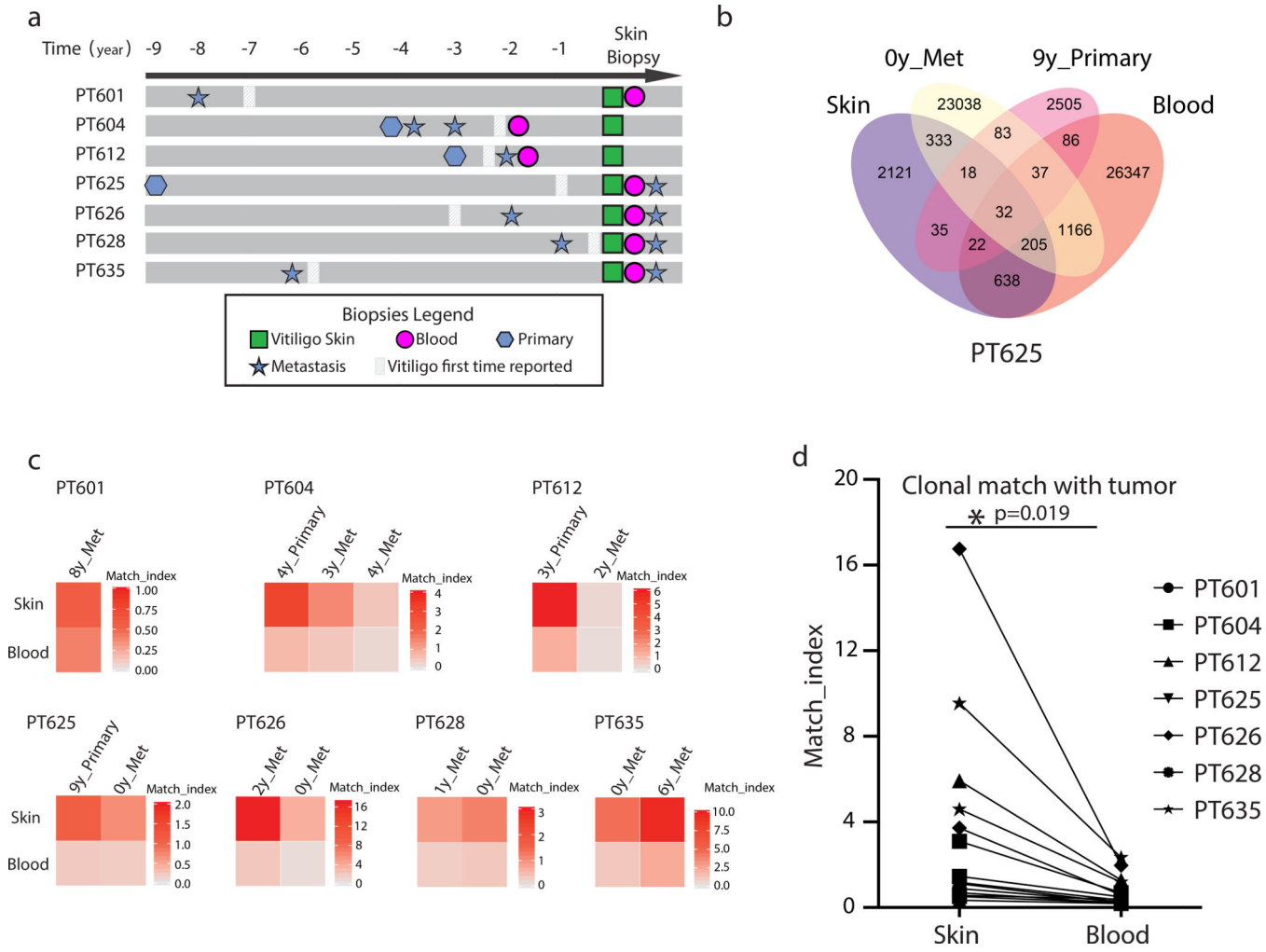

Figure 5: Tumor-associated T cell clonotypes persist for up to nine years, with skin sustaining a focused repertoire.

(**a**) Timeline of patient specimen acquisitions (in years) prior to skin biopsy; all samples were analyzed by bulk TCRß CDR3 region DNA sequencing (**b**) Representative Venn diagram depicting number of tumor-associated clonotypes shared between tissues in one patient. (**c**) Heatmaps depicting clonal overlap, calculated as a match index (see Methods), between patient-matched tumor and skin or tumor and blood specimens. (**d**) Comparison of clonal overlap between tumor and skin vs. tumor and blood for individual tumor specimens. Lines link a single tumor specimen; with symbols representing different patients. Significance denotes overall difference in clonal match index between skin and blood, determined using N=14 tumor specimens taken from a total of 7 patients; $*P < 0.05$ by two-sided paired Student's t-test.

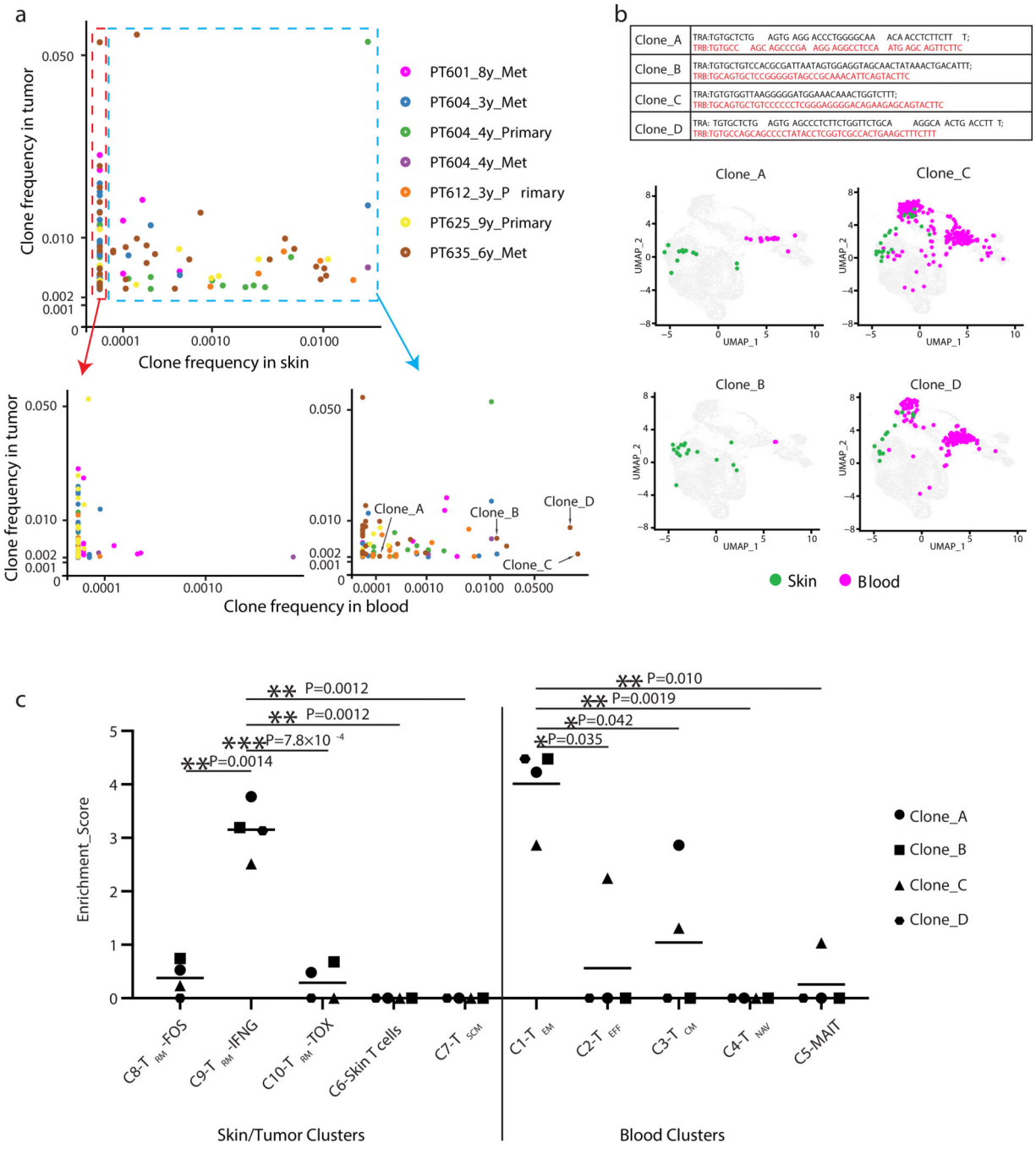

Figure 6: CD8$^+$ T cell clones from tumors persist as T_{RM} cells in skin and as T_{EM} cells in blood.

(**a**) Tumors were paired with blood and skin specimens taken at least three years subsequently, and were analyzed by bulk TCRß CDR3 region DNA sequencing. Scatter plots depict the expansion of persisting clonotypes in skin and blood that are matched to tumors. Clonal expansion in skin (top) and clonal expansion in blood (bottom), indicating that tumor-associated clonotypes that had expanded in skin were also highly expanded in blood (bottom right). Dots indicate individual clonotypes; colors represent different tumors. Labeled clones A, B, C, and D are four tumor-associated DNA clonotypes that could be

matched 6 years later to clonotypes in the scRNA-seq dataset from the skin and blood of PT635. (**b**) Fully reconstructed paired TCR sequences from these clones are shown in the table (top); red denotes perfectly matched CDR3 regions). UMAP plots (bottom) indicate cluster distribution of these four long-persisting clonotypes in the single cell RNA-seq dataset from skin and blood of N=1 patient (PT635), with dots representing individual cells and colors denoting tissue of distribution. (**c**) Distribution of N=4 long-persisting TCR clonotypes from N=1 patient (PT635) among transcriptional clusters in the skin and blood. Points represent individual clonotypes, and lines indicate average enrichment scores, showing significance in differences of enrichment scores of all four clonotypes across the indicated clusters; $^{**}P < 0.01$ and $^{***}P < 0.001$ by two-sided paired Student's t-test.